Quantum Reaction Rates in Nonlinear Dissipative Systems
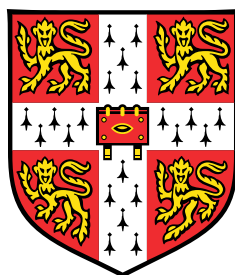
Oli Bridge

Department of Chemistry
University of Cambridge

Part III Project

St Catharine's College

April 2023

Declaration

This dissertation is submitted in partial fulfilment of the requirements for Part III Chemistry. It describes work carried out in the Department of Chemistry in the Michaelmas Term 2022 and the Lent Term 2023. Unless otherwise indicated, the research described is my own and not the product of collaboration.

Oli Bridge

April 2023

Acknowledgements

I would like to thank Professor Stuart Althorpe for his support and insight over the course of the project. I am also incredibly grateful for the guidance of Yair Litman throughout the year, who has always been willing to dedicate his time to answer my questions and talk through my findings. Lastly, my thanks go to Chris Haggard for many useful discussions, and to the rest of the Althorpe group for creating such a welcoming and inspiring atmosphere.

Abstract

Low energy excitations of electron-hole pairs in metals induce spatially-dependent non-adiabatic effects (NAEs) by coupling the nuclear and electronic degrees of freedom. It has recently been proposed that one can model this with a system nonlinearly coupled to a bath of harmonic oscillators. Additionally, systems involving light atoms exhibit significant nuclear quantum effects (NQEs), which may be accounted for with ring polymer molecular dynamics (RPMD), a method for simulating approximate quantum dynamics that conserves the quantum Boltzmann distribution. In this work, we investigate how the quantum rate in a one-dimensional double-well potential is affected by position-dependent friction. Numerical calculations show that the recrossing dynamics, which behave classically at room temperature, are significantly affected by the nonlinear friction. For strong coupling, quantum effects on the rate are also observed since the free energy contribution from the bath becomes strongly dependent on position. In the deep-tunnelling regime, a systematic lowering of the instanton crossover temperature with bath friction is observed to heavily impact the free energy barriers for both linear and nonlinear coupling. Extension of this model to a one-dimensional treatment of hydrogen hopping in bulk palladium shows that the inclusion of NAEs yields increases in the rate, primarily due to altered recrossing, that are greater than from the inclusion of NQEs.

Contents

Introduction

The computational study of dynamical properties in the condensed phase has been a popular area of research in theoretical chemistry for many years. Molecular dynamics (MD) is a widely used method which is able to calculate quantities such as time-correlation functions (TCFs) to good accuracy for certain systems, by treating the nuclei entirely classically. However, there are numerous systems in which a purely classical picture fails to describe its behaviour due to the presence of nuclear quantum effects (NQEs); these include zero-point energies[1] and quantum tunnelling[2,3]. For example, proton transfer reactions[4,5] and systems involving hydrogen self-diffusion[6] exhibit significant NQEs which must be accounted for in simulations. For condensed phase systems which typically involve many degrees of freedom, it quickly becomes too expensive to directly solve the Schrödinger equation. Alternatively, methods based on the Feynman path integral, such as path integral molecular dynamics (PIMD)[7,8], scale more favourably and are able to compute exact quantum time-independent properties. For time-dependent properties, approximate quantum dynamics methods have been developed that conserve quantum Boltzmann statistics and propagate the system using classical dynamics, which work well in the condensed phase due to fast quantum decoherence[9].

Popular dynamics methods based on the path integral formalism include centroid molecular dynamics (CMD)[10,11] and ring polymer molecular dynamics (RPMD)[12]. Although these were both developed as heuristic techniques, it has now been shown that they are approximations of a rigorous Boltzmann-conserving semiclassical theory called Matsubara dynamics[13,14]. RPMD has been extensively used in the calculation of reaction rates[4,5,15] by approximating the quantum flux-side correlation function, and has also been shown to be equivalent to an approximate form of semiclassical instanton theory[3,16], which explains its strong performance in the deep-tunnelling regime.

For systems involving light atoms diffusing through metals, non-adiabatic effects (NAEs) are present as well as NQEs. These are caused by low energy electron-hole pair excitations which couple the electronic and nuclear degrees of freedom within the material[17]. The Born-Oppenheimer approximation, which assumes the electrons reach a steady state on a much faster timescale than that of nuclear motion, breaks down for such systems[18]. NAEs can be modelled by a spatially-dependent 'electronic friction' exerted

on the nuclei[19], which has been observed in molecular beam scattering experiments[20] and in the vibrational relaxation of molecules adsorbed to surfaces[21]. In order to capture NAEs, one can use a modified version of the system-bath model, initially proposed by Caldeira and Leggett[22], where the linear coupling to the bath is replaced by a general nonlinear function, resulting in a position-dependent energy dissipation. Such a model has been previously studied for the rate of classically activated processes[23–25], which show that the spatial-dependence of the bath friction affects the recrossing dynamics. Recently, the ring polymer instanton with explicit friction (RPI-EF)[18] method has been developed which uses the nonlinear system-bath and approximates quantum rates at low temperatures. It has been shown to work well for medium to high friction strengths[26], but may only be employed below the instanton crossover temperature, where the reaction becomes dominated by deep tunnelling[3].

In this work, we use a nonlinear RPMD system-bath model for a one-dimensional double well potential, to capture NAEs and NQEs at any temperature. The project seeks to provide insight into the behaviour of the quantum rate with position-dependent friction. We apply this model to the electronic friction formalism by investigating the importance of including nonlinear coupling in calculations of the rate of hydrogen hopping in bulk palladium at room temperature.

This thesis is organised as follows. Part I outlines the relevant background theory for this work. In Part II, Chapter 4 presents the results for the nonlinear system-bath model, and Chapter 5 contains those for palladium. Chapter 6 gives a brief summary of our work and suggests directions for further research.

Part I

Theoretical Background

Chapter 1

Ring Polymer Molecular Dynamics

Ring polymer molecular dynamics (RPMD), developed by Craig and Manolopoulos[12], combines quantum Boltzmann statistics with classical dynamics using the Feynman path integral formulation of quantum mechanics[27]. It includes nuclear quantum effects (NQEs) by recasting each quantum degree of freedom into N copies of itself, connected by harmonic springs. This is known as the classical isomorphism[7,28]. RPMD treats the dynamics of these ring polymers literally in order to calculate time-dependent system properties[6,15,29].

In this chapter, we introduce static and dynamic statistical mechanical properties in classical and quantum form, and present a derivation of the ring polymer Hamiltonian.

1.1 Classical Statistical Mechanics

The classical Hamiltonian for an f-dimensional system is given by[30]

$$H(\mathbf{p}, \mathbf{q}) = \sum_{i=1}^{f} \frac{p_i^2}{2m_i} + V(\mathbf{q}). \tag{1.1}$$

It is possible to define the thermal average of a quantity $A(\mathbf{p}, \mathbf{q})$ as an integral over classical phase space:

$$\langle A \rangle = \frac{1}{(2\pi\hbar)^f Z_{\mathrm{cl}}} \int \mathrm{d}\mathbf{p} \int \mathrm{d}\mathbf{q} \, e^{-\beta H(\mathbf{p}, \mathbf{q})} A(\mathbf{p}, \mathbf{q}), \tag{1.2}$$

where $\beta \equiv 1/k_B T$, $\int \mathrm{d}\mathbf{p} \equiv \int \mathrm{d}p_1 \ldots \mathrm{d}p_f$ and $\int \mathrm{d}\mathbf{q} \equiv \int \mathrm{d}q_1 \ldots \mathrm{d}q_f$. The classical partition function, Z_{cl}, is given by

$$Z_{\mathrm{cl}} = \frac{1}{(2\pi\hbar)^f} \int \mathrm{d}\mathbf{p} \int \mathrm{d}\mathbf{q} \, e^{-\beta H(\mathbf{p}, \mathbf{q})}. \tag{1.3}$$

The thermal average of A is a time-independent property. Time-dependent properties, such as time-correlation functions (TCFs), are also of interest as they provide information on the dynamics of a system. The classical TCF can be written as:

$$c_{AB}(t) = \langle A(0)B(t)\rangle = \frac{1}{(2\pi\hbar)^f Z_{\mathrm{cl}}} \int \mathrm{d}\mathbf{p} \int \mathrm{d}\mathbf{q} \, \mathrm{e}^{-\beta H(\mathbf{p},\mathbf{q})} A(\mathbf{p},\mathbf{q}) B(\mathbf{p}_t,\mathbf{q}_t). \tag{1.4}$$

In the classical TCF, the property A depends on the initial phase space coordinates $(\mathbf{p},\mathbf{q})$, and the property B depends on the phase space coordinates after time t. It can be shown that the classical TCF obeys various symmetries, such as detailed balance and time translational invariance[30].

1.2   Quantum Statistical Mechanics

Now we consider the following quantum Hamiltonian:

$$\hat{H} = \frac{\hat{p}^2}{2m} + V(\hat{q}), \tag{1.5}$$

where $\hat{p}$ and $\hat{q}$ are the one-dimensional position and momentum operators. The expectation value of the quantum operator $\hat{A}$ is given by a trace over any complete orthonormal basis set, $\{|\phi_k\rangle\}$, of the Hilbert space[31]:

$$\langle A \rangle = \sum_k \langle \phi_k | \hat{\rho}\hat{A} | \phi_k \rangle = \mathrm{Tr}\left[\hat{\rho}\hat{A}\right], \tag{1.6}$$

where $\hat{\rho} = \sum_j P_j |\psi_j\rangle \langle\psi_j|$ is the density operator. Given the thermal density operator[31] $\hat{\rho}_{\mathrm{eq}} = \frac{1}{Z}\mathrm{e}^{-\beta\hat{H}}$, the thermal average of a quantum observable is

$$\langle A \rangle = \frac{1}{Z}\mathrm{Tr}\left[\mathrm{e}^{-\beta\hat{H}}\hat{A}\right], \tag{1.7}$$

where the quantum partition function, Z, is given by the trace of the Boltzmann operator:

$$Z = \mathrm{Tr}\left[\mathrm{e}^{-\beta\hat{H}}\right]. \tag{1.8}$$

One can also evaluate dynamic properties such as TCFs for quantum systems. The standard quantum TCF is written as[32]

$$C_{AB}(t) = \frac{1}{Z}\mathrm{Tr}\left[\mathrm{e}^{-\beta\hat{H}}\hat{A}\,\mathrm{e}^{+i\hat{H}t/\hbar}\hat{B}\mathrm{e}^{-i\hat{H}t/\hbar}\right], \tag{1.9}$$

where $\mathrm{e}^{+i\hat{H}t/\hbar}\hat{B}\mathrm{e}^{-i\hat{H}t/\hbar} = \hat{B}(t)$ is the time-evolved form of $\hat{B}$ in the Heisenberg picture[33]. Standard quantum TCFs do not have very many useful symmetry properties[12]. A much

more practical form of the quantum TCF is the Kubo-transformed correlation function[34] which is given by

$$\tilde{C}_{AB}(t) = \frac{1}{\beta Z} \int_0^\beta d\lambda \, \mathrm{Tr} \left[e^{-(\beta-\lambda)\hat{H}} \hat{A} e^{-\lambda\hat{H}} \, e^{+i\hat{H}t/\hbar} \hat{B} e^{-i\hat{H}t/\hbar} \right]. \tag{1.10}$$

Kubo-transformed TCFs possess the same symmetries as classical TCFs[12] and are therefore more useful for examining quantum properties using methods that combine quantum statistics and classical dynamics. The standard and Kubo-transformed quantum TCFs are related through their Fourier transforms[12].

1.3   The Classical Isomorphism

We start by considering the Hamiltonian in Equation (1.5) and expressing Equation (1.8) in position space:

$$Z = \int dq \, \langle q | e^{-\beta\hat{H}} | q \rangle. \tag{1.11}$$

The Boltzmann operator cannot be easily factorised since the kinetic and potential energy operators $\hat{T}$ and $\hat{V}$ do not commute. Instead, one may split up the Boltzmann operator using a Trotter factorisation[30], which is exact in the limit $N \to \infty$:

$$e^{-\beta\hat{H}} = e^{-\beta(\hat{T}+\hat{V})} = \lim_{N\to\infty} \left(e^{-\beta_N\hat{V}/2} \, e^{-\beta_N\hat{T}} \, e^{-\beta_N\hat{V}/2} \right)^N, \tag{1.12}$$

where $\beta_N = \beta/N$. By taking this factorisation form with finite N, inserting $N-1$ resolutions of the identity[33], $\int dq_j \, |q_j\rangle \langle q_j|$, and relabelling $q \to q_1$, one can define the following quantity[30]:

$$Z_N = \int dq_1 \ldots dq_N \, \langle q_1 | e^{-\beta_N\hat{V}/2} \, e^{-\beta_N\hat{T}} \, e^{-\beta_N\hat{V}/2} | q_2 \rangle \ldots \langle q_N | e^{-\beta_N\hat{V}/2} \, e^{-\beta_N\hat{T}} \, e^{-\beta_N\hat{V}/2} | q_1 \rangle. \tag{1.13}$$

One can evaluate the matrix elements appearing in Equation (1.13) as follows:

$$\langle q_j | e^{-\beta_N\hat{V}/2} \, e^{-\beta_N\hat{T}} \, e^{-\beta_N\hat{V}/2} | q_{j+1} \rangle = e^{-\beta_N V(q_j)/2} \langle q_j | e^{-\beta_N\hat{p}^2/2m} | q_{j+1} \rangle e^{-\beta_N V(q_{j+1})/2}$$

$$= e^{-\frac{\beta_N}{2}[V(q_j)+V(q_{j+1})]} \int d\tilde{p}_j \, \langle q_j | e^{-\beta_N\hat{p}^2/2m} | \tilde{p}_j \rangle \langle \tilde{p}_j | q_{j+1} \rangle. \tag{1.14}$$

In the first line the potential operator is applied to the eigenstates $|q_j\rangle$ and $|q_{j+1}\rangle$, and in the second line an identity in the momentum basis[33] has been inserted. Next, the kinetic energy operator is applied to the eigenstate $|\tilde{p}_j\rangle$, and the relation $\langle p|q \rangle = e^{-ipq/\hbar}/\sqrt{2\pi\hbar}$[33]

is used to obtain:

$$\langle q_j | e^{-\beta_N \hat{V}/2} \, e^{-\beta_N \hat{T}} \, e^{-\beta_N \hat{V}/2} | q_{j+1} \rangle = e^{-\frac{\beta_N}{2}[V(q_j)+V(q_{j+1})]} \frac{1}{2\pi\hbar} \int d\tilde{p}_j \, e^{-\beta_N \tilde{p}_j^2/2m} \, e^{i\tilde{p}_j(q_j-q_{j+1})/\hbar}. \tag{1.15}$$

Finally, completing the square on the exponents of the integrand, and performing the change in variable $p_j = \tilde{p}_j - im\omega_N(q_j - q_{j+1})$, where $\omega_N = 1/\beta_N\hbar$, gives

$$\langle q_j | e^{-\beta_N \hat{V}/2} \, e^{-\beta_N \hat{T}} \, e^{-\beta_N \hat{V}/2} | q_{j+1} \rangle = e^{-\frac{\beta_N}{2}[V(q_j)+V(q_{j+1})+m\omega_N^2(q_j-q_{j+1})^2]} \frac{1}{2\pi\hbar} \int dp_j \, e^{-\beta_N p_j^2/2m}. \tag{1.16}$$

Substituting this back into Equation (1.13) yields the result:

$$Z_N = \frac{1}{(2\pi\hbar)^N} \int d\mathbf{p} \int d\mathbf{q} \, e^{-\beta_N H_N(\mathbf{p},\mathbf{q})}, \tag{1.17}$$

where the N-bead ring polymer Hamiltonian is defined as

$$H_N(\mathbf{p},\mathbf{q}) = \sum_{j=1}^{N} \left[\frac{p_j^2}{2m} + \frac{1}{2}m\omega_N^2(q_j - q_{j+1})^2 + V(q_j) \right], \tag{1.18}$$

with $q_{N+j} \equiv q_j$ (cyclic boundary conditions). The link between the quantum partition function and a classical ring polymer connected by harmonic springs is known as the classical isomorphism†. By treating the ring polymer as an extended classical phase space, one can form an estimator for the average of an observable, A. For a position-dependent operator, $A(\hat{q})$, the ring polymer thermal average is given by[12]

$$\langle A \rangle_N = \frac{1}{(2\pi\hbar)^N Z_N} \int d\mathbf{p} \int d\mathbf{q} \, e^{-\beta_N H_N(\mathbf{p},\mathbf{q})} A_N(\mathbf{q}), \tag{1.19}$$

where $A_N(\mathbf{q})$ is defined as:

$$A_N(\mathbf{q}) = \frac{1}{N} \sum_{j=1}^{N} A(q_j). \tag{1.20}$$

These equilibrium properties are exact in the infinite-bead limit ($\langle A \rangle = \lim_{N\to\infty} \langle A \rangle_N$). For dynamic properties, by evolving this fictitious system in time, ring polymers can be used to *approximate* the Kubo-transformed quantum TCF due to its classical symmetries:

$$\tilde{C}_{AB}^{(N)}(t) = \langle A(0)B(t) \rangle_N = \frac{1}{(2\pi\hbar)^N Z_N} \int d\mathbf{p} \int d\mathbf{q} \, e^{-\beta_N H_N(\mathbf{p},\mathbf{q})} A_N(\mathbf{q}) B_N(\mathbf{q}_t). \tag{1.21}$$

This method is known as RPMD[12]. The ring polymer TCF is exact only in the infinite-bead limit when $t \to 0$. Another useful property of the ring polymers is that it is possible

---

†See Appendix A for an alternative derivation from path integral theory.

to cast its Hamiltonian into normal mode coordinates via a discrete Fourier transform. They are given by[35]:

$$P_k = \sum_{j=1}^{N} C_{jk} p_j \qquad Q_k = \sum_{j=1}^{N} C_{jk} q_j, \tag{1.22}$$

where (for even N),

$$C_{jk} = \begin{cases} \sqrt{1/N} & k = 0 \\ \sqrt{2/N} \cos(2\pi jk/N) & 1 \le k \le N/2 - 1 \\ \sqrt{1/N}(-1)^j & k = N/2 \\ \sqrt{2/N} \sin(2\pi jk/N) & N/2 + 1 \le k \le N - 1 \end{cases} \tag{1.23}$$

The normal mode frequencies are given by $\omega_k = 2\omega_N \sin(k\pi/N)$. Using this basis proves very useful in the computational implementation of evolving the ring polymer dynamics in time.[†]

[†]See Appendix D for computational details of the RPMD simulations.

Chapter 2

Quantum Rate Theory

Thermal rate constants are important quantities in the study of quantum dynamics and are the key computed results in this work. This chapter demonstrates how quantum rates can be approximated using RPMD, and how the rare-event nature of a reactive crossing can be circumvented in the calculation of rate constants.

The exact quantum mechanical rate constant at temperature T can be written as[36,37]

$$k(T) = \frac{1}{Q_r(T)} \lim_{t\to\infty} \widetilde{C}_{fs}(t), \tag{2.1}$$

where $Q_r(T)$ is the reactant partition function per unit length (for a one-dimensional barrier problem), and $\widetilde{C}_{fs}(t)$ is the Kubo-transformed flux-side correlation function[15,29]:

$$\widetilde{C}_{fs}(t) = \frac{1}{\beta} \int_0^\beta d\lambda \, \mathrm{Tr}\left[e^{-(\beta-\lambda)\hat{H}} \hat{F} e^{-\lambda\hat{H}} \, e^{+i\hat{H}t/\hbar} \hat{h} e^{-i\hat{H}t/\hbar} \right]. \tag{2.2}$$

The flux operator is given by

$$\hat{F} = \frac{i}{\hbar}\left[\hat{H}, \hat{h}\right]. \tag{2.3}$$

where $[\,\cdot\,,\,\cdot\,]$ is the commutator. The operator $\hat{h} = h(\hat{q} - q^{\ddagger})$, where $h(q)$ is the Heaviside step function, projects onto the product side of some dividing surface $q^{\ddagger}$. Equation (2.1) holds for both standard and Kubo-transformed flux-side TCFs[29]; the use of the latter shows it is possible to approximate rates with RPMD, as the following sections outline.

2.1 RPMD Rate Theory

The ring polymer approximation to the rate constant is given by[4,15]

$$k^{(N)}(T) = \frac{1}{Q_r^{(N)}(T)} \lim_{t\to\infty} \widetilde{C}_{fs}^{(N)}(t), \tag{2.4}$$

The ring polymer flux-side TCF, $\widetilde{C}_{fs}^{(N)}(t)$, is given by

$$\widetilde{C}_{fs}^{(N)}(t) = \frac{1}{(2\pi\hbar)^{Nf}} \int \mathrm{d}^{Nf}\mathbf{p} \int \mathrm{d}^{Nf}\mathbf{q}\, e^{-\beta_N H_N(\mathbf{p},\mathbf{q})} \delta[\bar{s}(\mathbf{q})] \bar{v}_s(\mathbf{p},\mathbf{q}) h[\bar{s}(\mathbf{q}_t)] \qquad (2.5)$$

for an f-dimensional system with N ring polymer beads per degree of freedom, and

$$Q_r^{(N)}(T) = \frac{1}{(2\pi\hbar)^{Nf}} \int \mathrm{d}^{Nf}\mathbf{p} \int \mathrm{d}^{Nf}\mathbf{q}\, e^{-\beta_N H_N(\mathbf{p},\mathbf{q})} h[-\bar{s}(\mathbf{q})] \qquad (2.6)$$

is the reactant partition function per unit volume. The transition state dividing surface, $\bar{s}(\mathbf{q})$, is defined as $\bar{s}(\mathbf{q}) = s(\bar{q}_1, ..., \bar{q}_f) = 0$. The initial velocity along the reaction coordinate, the position centroid and the momentum centroid are defined as follows:

$$\bar{v}_s(\mathbf{p},\mathbf{q}) = \sum_{i=1}^{f} \frac{\partial \bar{s}(\mathbf{q})}{\partial \bar{q}_i} \frac{\bar{p}_i}{m_i}, \qquad (2.7)$$

$$\bar{q}_i = \frac{1}{N} \sum_{j=1}^{N} q_{i,j} \qquad \bar{p}_i = \frac{1}{N} \sum_{j=1}^{N} p_{i,j}. \qquad (2.8)$$

When the reaction coordinate is one of the Cartesian coordinates, q_s, the transition state dividing surface may be expressed as $\bar{s}(\mathbf{q}) = q_s^{\ddagger} - \bar{q}_s$, and $\widetilde{C}_{fs}^{(N)}(t)$ can be rewritten into a simpler form[4] which shall be considered for the remainder of the chapter:

$$\widetilde{C}_{fs}^{(N)}(t) = \frac{1}{(2\pi\hbar)^{Nf}} \int \mathrm{d}^{Nf}\mathbf{p} \int \mathrm{d}^{Nf}\mathbf{q}\, e^{-\beta_N H_N(\mathbf{p},\mathbf{q})} \delta(q_s^{\ddagger} - \bar{q}_s)(\bar{p}_s/m_s) h(\bar{q}_s(t) - q_s^{\ddagger}). \quad (2.9)$$

The transition state theory (TST) rate neglects any recrossing dynamics, and can be calculated from the instantaneous flux through the dividing surface, provided by the zero-time limit of the flux-side TCF. The RPMD TST rate is therefore given by:

$$k^{\mathrm{QTST}}(T) = \frac{1}{Q_r^{(N)}(T)} \lim_{t\to 0^+} \widetilde{C}_{fs}^{(N)}(T). \qquad (2.10)$$

The zero-time limit of $\widetilde{C}_{fs}^{(N)}(t)$ can be written as[29]:

$$\lim_{t\to 0^+} \widetilde{C}_{fs}^{(N)}(t) = \frac{1}{(2\pi\beta m_s)^{1/2}} \frac{1}{(2\pi\hbar)^{Nf}} \int \mathrm{d}^{Nf}\mathbf{p} \int \mathrm{d}^{Nf}\mathbf{q}\, e^{-\beta_N H_N(\mathbf{p},\mathbf{q})} \delta(q_s^{\ddagger} - \bar{q}_s), \qquad (2.11)$$

By defining the forward classical flux through the dividing surface, $\frac{1}{2}\langle |\dot{q}_s| \rangle_{\mathrm{cl}}$, and the centroid-constrained partition function, $Q^{(N)}(q_s^{\ddagger})$,

$$\frac{1}{2}\langle |\dot{q}_s| \rangle_{\mathrm{cl}} = \frac{1}{(2\pi\beta m_s)^{1/2}}, \qquad (2.12)$$

and

$$Q^{(N)}(q_s^\ddagger) = \frac{1}{(2\pi\hbar)^{Nf}} \int \mathrm{d}^{Nf}\mathbf{p} \int \mathrm{d}^{Nf}\mathbf{q} \, e^{-\beta_N H_N(\mathbf{p},\mathbf{q})} \delta(q_s^\ddagger - \bar{q}_s), \tag{2.13}$$

one can express the RPMD transition state theory rate constant in the form[†],

$$k^{\mathrm{QTST}}(T) = \frac{1}{2}\langle|\dot{q}_s|\rangle_{\mathrm{cl}} \frac{Q^{(N)}(q_s^\ddagger)}{Q_r^{(N)}(T)} = \frac{1}{2}\langle|\dot{q}_s|\rangle_{\mathrm{cl}} \frac{\langle\delta(q_s^\ddagger - \bar{q}_s)\rangle}{\langle h(q_s^\ddagger - \bar{q}_s)\rangle}. \tag{2.14}$$

2.2 Bennett-Chandler Method

The Bennett-Chandler method[4,38,39] is a useful method for computing rate constants when the event of a reactive crossing is rare. We start by expressing the RPMD rate coefficient of Equation (2.4) in terms of thermal averages:

$$k^{(N)}(T) = \lim_{t\to\infty} \frac{\langle\delta(q_s^\ddagger - \bar{q}_s)(\bar{p}_s/m)h(\bar{q}_s(t) - q_s^\ddagger)\rangle}{\langle h(q_s^\ddagger - \bar{q}_s)\rangle}. \tag{2.15}$$

Multiplying the numerator and denominator by $\frac{1}{2}\langle|\dot{q}_s|\rangle_{\mathrm{cl}}\langle\delta(q_s^\ddagger - \bar{q}_s)\rangle$ gives

$$k^{(N)}(T) = \lim_{t\to\infty} \frac{1}{2}\langle|\dot{q}_s|\rangle_{\mathrm{cl}} \frac{\langle\delta(q_s^\ddagger - \bar{q}_s)\rangle}{\langle h(q_s^\ddagger - \bar{q}_s)\rangle} \frac{\langle\delta(q_s^\ddagger - \bar{q}_s)(\bar{p}_s/m_s)h(\bar{q}_s(t) - q_s^\ddagger)\rangle}{\frac{1}{2}\langle|\dot{q}_s|\rangle_{\mathrm{cl}}\langle\delta(q_s^\ddagger - \bar{q}_s)\rangle}, \tag{2.16}$$

which allows the rate coefficient of a condensed phase system to be expressed as a product of two terms[4]:

$$k^{(N)}(T) = \kappa(\tau_p)k^{\mathrm{QTST}}(T), \tag{2.17}$$

where τ_p is the plateau time, and $k^{\mathrm{QTST}}(T)$ is defined in Equation (2.14). Using the fact that $\langle\delta(q^\ddagger - \bar{q})(\bar{p}/m)h(\bar{p})\rangle = \frac{1}{2}\langle|\dot{q}|\rangle_{\mathrm{cl}}\langle\delta(q^\ddagger - \bar{q})\rangle$ (see Appendix B.1), the transmission coefficient, $\kappa(t)$, is defined as:

$$\kappa(t) = \frac{\langle\delta(q_s^\ddagger - \bar{q}_s)(\bar{p}_s/m_s)h(\bar{q}_s(t) - q_s^\ddagger)\rangle}{\langle\delta(q_s^\ddagger - \bar{q}_s)(\bar{p}_s/m_s)h(\bar{p}_s)\rangle}. \tag{2.18}$$

This can be straightforwardly computed in an RPMD simulation by thermalising each trajectory with the system ring polymer centroid constrained to $\bar{q}_s = q_s^\ddagger$, subsequently evolving the trajectory without constraint, and averaging contributions of the top and bottom of Equation (2.18). For a condensed phase system, further reactive crossings over longer timescales cause $\kappa(t)$ to eventually decay to zero. Thus, $\kappa(t)$ is evaluated when it reaches its initial plateau at $t = \tau_p$, rather than for $t \to \infty$[4]. Evaluating $k^{\mathrm{QTST}}(T)$ in the form of Equation (2.14) is often impractical, since the reaction coordinate is rarely

---

[†]See Appendix B.1 for a full derivation of RPMD TST from the zero-time limit of $\widetilde{C}_{fs}^{(N)}(t)$.

at the top of the barrier ($\bar{q}_s = q_s^{\ddagger}$). To allow for efficient evaluation of $k^{\mathrm{QTST}}(T)$, we define the probability of the ring polymer centroid being at q_s' to be

$$p(q_s') = \frac{\langle \delta(q_s' - \bar{q}_s) \rangle}{\langle h(q_s^{\ddagger} - \bar{q}_s) \rangle}. \tag{2.19}$$

The corresponding free energy function is

$$\mathcal{F}(q_s') = -\frac{1}{\beta} \ln p(q_s'), \tag{2.20}$$

and the probability of finding the ring polymer centroid at $q_s^{\ddagger}$ can be written as

$$p(q_s^{\ddagger}) = p(q_s^0) \, \exp\left(-\beta \left[\mathcal{F}(q_s^{\ddagger}) - \mathcal{F}(q_s^0)\right]\right)$$

$$= p(q_s^0) \, \exp\left(-\beta \int_{q_s^0}^{q_s^{\ddagger}} \mathrm{d}q_s' \, \frac{\mathrm{d}\mathcal{F}(q_s')}{\mathrm{d}q_s'}\right). \tag{2.21}$$

The value of q_s^0 is chosen to lie in the highly populated reactant region. The free energy derivative inside in the integral in Equation (2.21) is calculated from the centroid-constrained mean force[†]:

$$\frac{\mathrm{d}\mathcal{F}(q_s')}{\mathrm{d}q_s'} = \left\langle \frac{1}{N} \sum_{j=1}^{N} \frac{\partial V(q_j)}{\partial q_j} \right\rangle_{\bar{q}_s = q_s'}, \tag{2.22}$$

where the centroid-constrained average over the canonical ensemble is given by:

$$\langle ... \rangle_{q_s'} = \frac{\int \mathrm{d}^{Nf} \mathbf{p} \int \mathrm{d}^{Nf} \mathbf{q} \, \mathrm{e}^{-\beta_N H_N(\mathbf{p},\mathbf{q})} \delta(q_s' - \bar{q}_s)(...)}{\int \mathrm{d}^{Nf} \mathbf{p} \int \mathrm{d}^{Nf} \mathbf{q} \, \mathrm{e}^{-\beta_N H_N(\mathbf{p},\mathbf{q})} \delta(q_s' - \bar{q}_s)}, \tag{2.23}$$

for f Hamiltonian degrees of freedom and N ring polymer beads per degree of freedom. The RPMD TST rate constant can therefore be recast to

$$k^{\mathrm{QTST}}(T) = \frac{1}{2} \langle |\dot{q}_s| \rangle_{\mathrm{cl}} \, p(q_s^{\ddagger}). \tag{2.24}$$

In practice, the $p(q_s^{\ddagger})$ term (from Equation (2.21)) is calculated in two parts[4]. Firstly, $p(q_s^0)$ is calculated from a histogram of an unconstrained simulation in the reactant well. The exponential term is then evaluated via thermodynamic integration by selecting a series of points between q_s^0 and $q_s^{\ddagger}$, computing a centroid-constrained mean force calculation for each point and numerically integrating the resulting values.

[†]See Appendix B.2 for a derivation of the mean force.

Chapter 3

Electronic Friction

The lack of band gap for metallic systems leads to energy exchange between the electrons and the nuclear degrees of freedom in the form of low-energy electronic excitations[17]. Such non-adiabatic effects (NAEs) can be modelled by subjecting the nuclei to a position-dependent electronic friction[18,19,21]. In order to model this computationally, it is instructive to consider nonlinear coupling to a harmonic bath[18,24,25,40], rather than a linear coupling[15,22,41]. In this chapter we outline the system-bath model with general coupling, its key properties and how it can be applied to electronic friction.

3.1 Nonlinear System-Bath Model

The classical Hamiltonian for general coupling $f_i(q)$ with N_b bathmodes is given by[40]

$$H(p, q, \mathbf{p}_b, \mathbf{x}) = \frac{p^2}{2\mu} + V(q) + \sum_{i=1}^{N_b} \left[\frac{p_i^2}{2m_i} + \frac{1}{2} m_i \omega_i^2 \left(x_i - \frac{f_i(q)}{m_i \omega_i^2} \right)^2 \right], \qquad (3.1)$$

where p and q are the system momentum and position, μ is the system mass, and p_i, x_i, m_i and ω_i are the momentum, position, mass and frequency for harmonic bathmode i. The corresponding RPMD system-bath Hamiltonian is written as

$$\begin{aligned} H_N(\mathbf{p}, \mathbf{q}, \mathbf{p}_b, \mathbf{x}) = &\sum_{j=1}^{N} \left[\frac{p_j^2}{2\mu} + \frac{1}{2} \mu \omega_N^2 \left(q_j - q_{j+1} \right)^2 + V(q_j) \right] \\ &+ \sum_{i=1}^{N_b} \sum_{j=1}^{N} \left[\frac{p_{i,j}^2}{2m_i} + \frac{1}{2} m_i \omega_N^2 \left(x_{i,j} - x_{i,j+1} \right)^2 + \frac{1}{2} m_i \omega_i^2 \left(x_{i,j} - \frac{f_i(q_j)}{m_i \omega_i^2} \right)^2 \right]. \end{aligned}$$

$$(3.2)$$

In this work, the position-dependence is introduced with separable coupling, where the system-bath interaction is written as a product of a frequency-dependent coefficient and

a position-dependent function[18,40]:

$$f_i(q) = c_i g(q). \tag{3.3}$$

The spectral density, which encodes the behaviour of the bath, is given by[18]

$$J(q, \omega) = \frac{\pi}{2} \left(\frac{\partial f_i(q)}{\partial q} \right)^2 \sum_{i=1}^{N_b} \frac{1}{m_i \omega_i} \, \delta(\omega - \omega_i)$$

$$= \frac{\pi}{2} \left(\frac{\partial g(q)}{\partial q} \right)^2 \sum_{i=1}^{N_b} \frac{c_i^2}{m_i \omega_i} \, \delta(\omega - \omega_i). \tag{3.4}$$

The corresponding time- and position-dependent friction kernel is related to the spectral density as follows:

$$\eta(q, t) = \frac{2}{\pi} \int_0^\infty d\omega \, \frac{J(q, \omega)}{\omega} \, \cos(\omega t), \tag{3.5}$$

with its frequency- and position-dependent Laplace transform defined as

$$\tilde{\eta}(q, \lambda) = \int_0^\infty dt \, e^{-\lambda t} \, \eta(q, t) = \frac{2}{\pi} \int_0^\infty d\omega \, \frac{J(q, \omega)}{\omega} \, \frac{\lambda}{\lambda^2 + \omega^2}. \tag{3.6}$$

In order to gain insight into the behaviour of the free energy with friction, one must evaluate the system-bath partition function. To do this, firstly the potential terms (including the spring terms) in Equation (3.2) are expressed in normal mode coordinates as follows:

$$V_N^{\text{sb}} = \sum_{k=0}^{N-1} \frac{1}{2} \mu \omega_k^2 Q_k^2 + \sum_{j=1}^{N} V(q_j) + \sum_{k=0}^{N-1} \sum_{i=1}^{N_b} \left[\frac{1}{2} m_i \omega_k^2 X_{i,k}^2 + \frac{1}{2} m_i \omega_i^2 \left(X_{i,k}^2 - \frac{F_{i,k}}{m_i \omega_i^2} \right)^2 \right], \tag{3.7}$$

where $F_{i,k} = \sum_{j=1}^{N} C_{jk} f_i(q_j)$ is the coordinate-transformed system-bath coupling. With some algebraic manipulation, V_N^{sb} can be re-expressed as[18]

$$V_N^{\text{sb}} = \overbrace{\sum_{k=0}^{N-1} \frac{1}{2} \mu \omega_k^2 Q_k^2 + \sum_{j=1}^{N} V(q_j)}^{V_N^{\text{sys}}} + \sum_{k=0}^{N-1} \sum_{i=1}^{N_b} \frac{1}{2} \frac{F_{i,k}^2 \, \omega_k^2}{m_i \omega_i^2 (\omega_i^2 + \omega_k^2)}$$

$$+ \sum_{k=0}^{N-1} \sum_{i=1}^{N_b} \frac{1}{2} m_i (\omega_i^2 + \omega_k^2) \left(X_{i,k}^2 - \frac{F_{i,k}}{m_i (\omega_i^2 + \omega_k^2)} \right)^2, \tag{3.8}$$

which allows the bath degrees of freedom to be integrated out in the partition function. Integrating out all the momenta and the bath positions yields the system-bath partition

function:

$$Z_N = Z_N^{\text{bath}} \left(\frac{\mu}{2\pi \beta_N \hbar^2} \right)^{N/2} \int d\mathbf{q} \, e^{-\beta_N V_N^{\text{eff}}}, \tag{3.9}$$

where

$$Z_N^{\text{bath}} = \prod_{i=1}^{N_b} \prod_{k=0}^{N-1} \frac{1}{\beta_N \hbar \sqrt{\omega_i^2 + \omega_k^2}} \qquad V_N^{\text{eff}} = V_N^{\text{sys}} + \sum_{i=1}^{N_b} \sum_{k=0}^{N-1} \frac{1}{2} \frac{\omega_k^2}{m_i \omega_i^2 (\omega_i^2 + \omega_k^2)} F_{i,k}^2. \tag{3.10}$$

For linear coupling, $f_i(q_j) = c_i q_j$, the coordinate-transformed coupling is given by $F_{i,k} = c_i Q_k$. The effective potential can be written as

$$V_N^{\text{eff}} = V_N^{\text{sys}} + \sum_{k=0}^{N-1} \left[\sum_{i=1}^{N_b} \frac{1}{2} \frac{\omega_k^2 \, c_i^2}{m_i \omega_i^2 (\omega_i^2 + \omega_k^2)} \right] Q_k^2$$

$$= V_N^{\text{sys}} + \sum_{k=0}^{N-1} \left[\frac{2}{\pi} \int_0^\infty d\omega \frac{J(\omega)}{\omega} \frac{\omega_k}{\omega^2 + \omega_k^2} \right] \frac{\omega_k}{2} Q_k^2 \tag{3.11}$$

$$= V_N^{\text{sys}} + \sum_{k=0}^{N-1} \frac{\tilde{\eta}(\omega_k) \omega_k}{2} Q_k^2,$$

where in the third line the Laplace transform of the friction kernel (Equation (3.6)) is recognised. The second term is defined as the renormalisation potential, which couples the fluctuation modes of the ring polymer. For a harmonic system potential ($V(q) = \frac{1}{2}\mu\omega^2 q^2$), the system positions can also be integrated out to give:

$$Z_N = Z_N^{\text{bath}} Z_N^{\text{eff}} = Z_N^{\text{bath}} \prod_{k=0}^{N-1} \frac{1}{\beta_N \hbar \sqrt{\omega^2 + \omega_k^2 + \frac{\tilde{\eta}(\omega_k)}{m} \omega_k}}, \tag{3.12}$$

and the corresponding free energy is given by

$$\mathcal{F} = -\frac{1}{\beta} \ln Z_N^{\text{bath}} - \frac{1}{\beta} \ln Z_N^{\text{eff}}. \tag{3.13}$$

The Laplace transform of the friction kernel, $\tilde{\eta}(\omega_k)$, gives a measure of the strength of coupling to the bath, so increasing the friction in the system-bath results in an increase in the free energy in the harmonic picture. This work seeks to determine if this relationship holds for nonlinear coupling, and what effect this has on the free energy barrier of a reaction.

3.2 Electronic Friction Tensor

For the NAEs present in metals, we consider the theory of electronic friction proposed by Head-Gordon and Tully[42]. The quadratic Hamiltonian for non-interacting electrons is given by[43]

$$\hat{H} = \sum_{pq} h_{qp}(\mathbf{q})\hat{a}_p^\dagger \hat{a}_q, \tag{3.14}$$

where p and q are the electronic orbital indices, $h_{qp}(\mathbf{q}) = \langle q|\hat{H}|p\rangle$ are the matrix elements which may depend on the nuclear coordinates $\mathbf{q}$, and $\hat{a}^\dagger$ and $\hat{a}$ are the fermion creation and annihilation operators. The electronic friction tensor is given by[18,44]

$$\eta_{ij}^{\text{el}}(\mathbf{q}, t) = -\text{Tr}_e\left[\partial_i\hat{H}e^{-i\hat{\mathcal{L}}t}\partial_j\hat{\rho}_{ss}\right], \tag{3.15}$$

where $\partial_i \equiv \partial/\partial q_i$, $\text{Tr}_e[\,\cdot\,]$ denotes a trace over the electronic degrees of freedom, $\hat{\mathcal{L}}$ is the Liouvillian superoperator, and $\hat{\rho}_{ss}$ is the steady state electronic density matrix[†]. The tensorial form of this expression specifies the components of the friction along all the nuclear degrees of freedom. It can be shown[18] that for the Hamiltonian in Equation (3.14) in the context of density functional theory (DFT), the friction tensor may be written in terms of Kohn-Sham states:

$$\eta_{ij}^{\text{el}}(\mathbf{q}, t) = \hbar \sum_{\nu,\nu'} \langle\psi_\nu|\partial_i\psi_{\nu'}\rangle\langle\psi_{\nu'}|\partial_j\psi_\nu\rangle\,\Omega_{\nu,\nu'}(f(\epsilon_\nu) - f(\epsilon_{\nu'}))\cos(\Omega_{\nu,\nu'}t), \tag{3.16}$$

where $f(\epsilon)$ is the Fermi-Dirac state occupation, $\Omega_{\nu,\nu'} = (\epsilon_{\nu'} - \epsilon_\nu)/\hbar$, and ψ_ν and ϵ_ν are the Kohn-Sham electronic orbitals and energies for state ν. By taking the Laplace transform of Equation (3.16), one can define the spectral density tensor that arises from electronic friction:

$$J_{ij}(\mathbf{q}, \omega) = \pi\hbar \sum_{\nu,\nu'} \langle\psi_\nu|\partial_i\psi_{\nu'}\rangle\langle\psi_{\nu'}|\partial_j\psi_\nu\rangle\,\omega^2(f(\epsilon_\nu) - f(\epsilon_{\nu'}))\delta(\omega - \Omega_{\nu,\nu'}). \tag{3.17}$$

This spectral density can be computed from *ab initio* DFT simulations at different positions along a reaction coordinate to form the position-dependent coupling to the nuclear degrees of freedom.

[†]See Appendix C for the origin of this expression.

Part II

Numerical Results

Chapter 4

Position-Dependent Friction

4.1 Nonlinear Coupling Model

In order to investigate the behaviour of a system nonlinearly coupled to a harmonic bath, the commonly used DW1 potential[45] was studied:

$$V(q) = -\frac{1}{2}m\omega_b^2 q^2 + \frac{m^2\omega_b^4}{16V_0^{\ddagger}}q^4, \tag{4.1}$$

where $m = m_p$, $\omega_b = 500\text{cm}^{-1}$ and $V_0^{\ddagger} = 2085\text{cm}^{-1}$. The system was studied with the separable coupling described in Chapter 3. The following position-dependent spectral density based on an Ohmic bath with exponential cut-off[15] was used:

$$J(q,\omega) = \left(\frac{\partial g(q;\epsilon)}{\partial q}\right)^2 \omega\, e^{-\omega/\omega_c}, \tag{4.2}$$

with $\omega_c = 500\text{cm}^{-1}$, where

$$g(q;\epsilon) = q\sqrt{\eta}\left(1 + \epsilon\, e^{-q^2/2}\right). \tag{4.3}$$

The value of η can be varied to change the coupling strength to the bath. In this work, two limiting cases of this function were examined for two values of the parameter ϵ:

$$g(q;\epsilon) = \begin{cases} q\sqrt{\eta} & \epsilon = 0 \quad \rightarrow \text{ linear} \\ q\sqrt{\eta}\left(1 - e^{-q^2/2}\right) & \epsilon = -1 \quad \rightarrow \text{ symmetric} \end{cases} \tag{4.4}$$

The 'linear' regime is that of a typical system-bath seen often in the literature[15,22]. The 'symmetric' regime gives the friction a position-dependence (see Fig. 4.1).
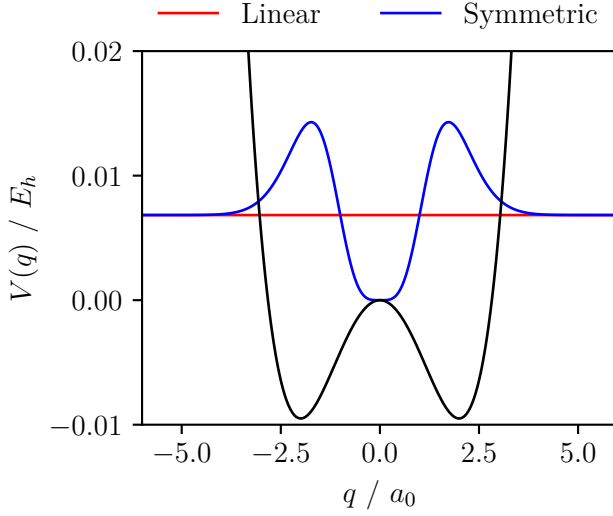
Fig. 4.1 DW1 potential energy surface (black) with corresponding plots of $(g'(q))^2$ to visualise the linear (red) and symmetric (blue) friction regimes. The y-units of the friction plots are arbitrary. Note that the friction is zero for symmetric friction at the transition state $q^{\ddagger}$, and tends to the linear regime for large q.

The bath frequencies and frequency-dependent coefficients are given by the following logarithmic discretisation:

$$\omega_i = -\omega_c \ln\left(\frac{i - 1/2}{N_b}\right) \qquad c_i = \omega_i \sqrt{\frac{2m_i\omega_c}{\pi N_b}}, \tag{4.5}$$

with $i = 1, \ldots, N_b$. These parameters can be determined analytically by the assumption that all bathmodes carry an equal fraction of the bath reorganisation energy[46].

4.2 Rate Calculations

Rate constants were calculated using both classical molecular dynamics and RPMD, with the Bennett-Chandler method described in Chapter 2[†]. Results were computed for $T = 300$K and $T = 50$K, for a range of values of the reduced system-bath coupling strength $\eta/m\omega_b$. Rates are reported in the form of the dimensionless constant κ, which is defined as the full rate constant divided by the classical TST rate:

$$\kappa = \frac{k^{(N)}(T)}{k_{\text{cl}}^{\text{TST}}(T)}, \tag{4.6}$$

where, for the DW1 potential, $k_{\text{cl}}^{\text{TST}}(T)$ can be well approximated by

$$k_{\text{cl}}^{\text{TST}}(T) \simeq \frac{\omega_b\sqrt{2}}{2\pi}\, e^{-\beta V_0^{\ddagger}}. \tag{4.7}$$

[†]See Appendix D for computational details.

4.2.1   Above the Crossover Temperature

At 300K, NQEs were observed to cause an increase in the RPMD rate from the classical values. This can be clearly seen in Fig. 4.2 for both linear and nonlinear regimes.
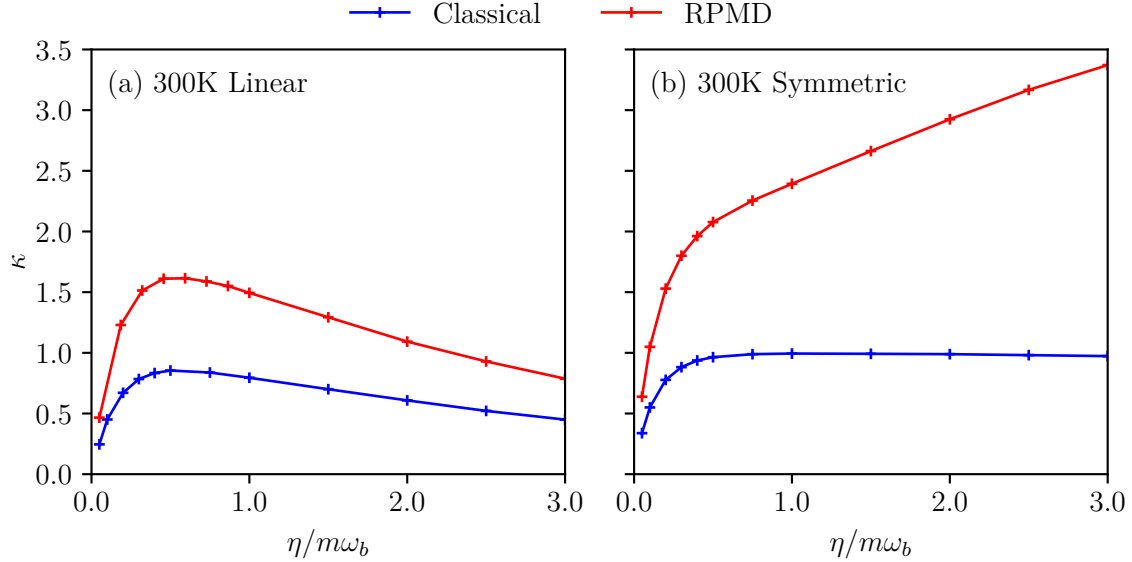

Fig. 4.2 Dimensionless rate constants at $T = 300$K. Panel (a) shows the linear friction regime and panel (b) shows the symmetric friction regime. In both cases, rates were computed from classical MD and RPMD with a fully converged number of beads ($N = 16$).

The linear friction results are in agreement with the results obtained by Craig and Manolopoulos for the same system[15]. In this case, the classical and RPMD rates follow a similar trend that is in agreement with Kramer's turnover theory[47]. For weak friction, an increase in the coupling strength increases the probability of a sufficiently strong kick from the bath to cause a reactive barrier crossing ($\kappa \propto \eta$). In the high friction limit, the bath interaction is so strong that there is heavy dissipation which damps many trajectories heading for the barrier. Thus, an increase in coupling strength will decrease the rate in this limit ($\kappa \propto 1/\eta$).

    Interesting results come from the symmetric regime, in which the classical rate tends to a maximum value of 1 (zero recrossing), whereas the RPMD rate is observed to systematically increase. This can be rationalised by examining the transmission and free energy components.

    It is clear from the similarity between the classical and RPMD transmission factors in Figs. 4.3 (a) and (b) that in both friction regimes at 300K, the ring polymer is sufficiently compact that the dynamics of its centroid behave classically.
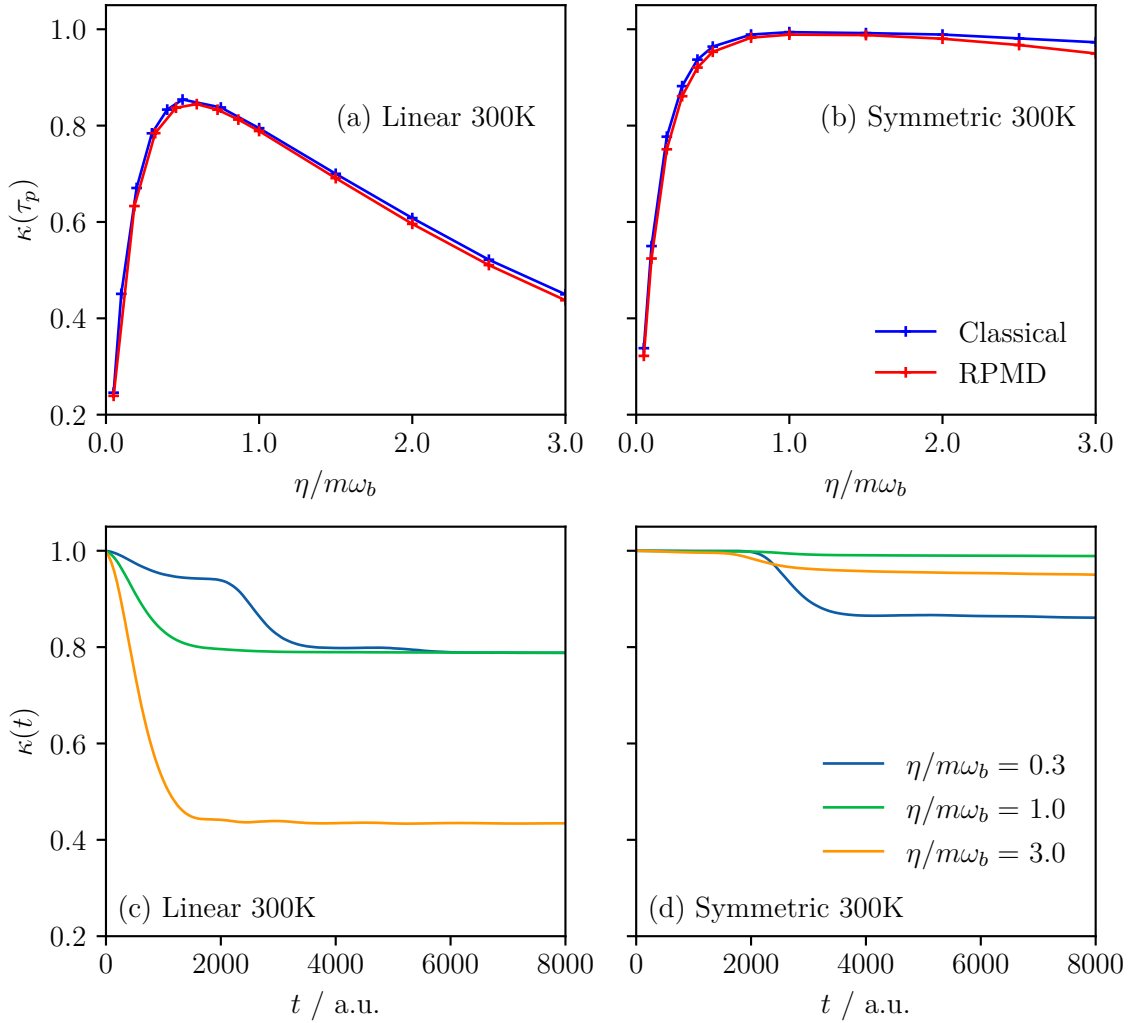
Fig. 4.3 Transmission coefficients at $T = 300$K. Panels (a) and (c) show results for linear friction; the former shows the value of $\kappa(\tau_p)$ as a function of $\eta/m\omega_b$ for classical MD and RPMD, whilst the latter shows the RPMD TCFs obtained for three selected $\eta/m\omega_b$ values. Panels (b) and (d) show the corresponding plots for symmetric friction.

Furthermore, Figs. 4.3 (c) and (d) demonstrate how the symmetric model permits much less recrossing, particularly for strong coupling. This is consistent with the nonlinear model exhibiting no friction at the barrier, causing most trajectories to fall into the wells which quickly dissipate their energy. The dynamics are therefore contributing to the increase in the rate from the linear to the symmetric regime.

However, the systematic increase seen in Fig. 4.2 (b) is attributed to the free energies, which are presented in Fig. 4.4. Both regimes exhibit lower free energy barriers than the classical case due to NQEs present at room temperature.
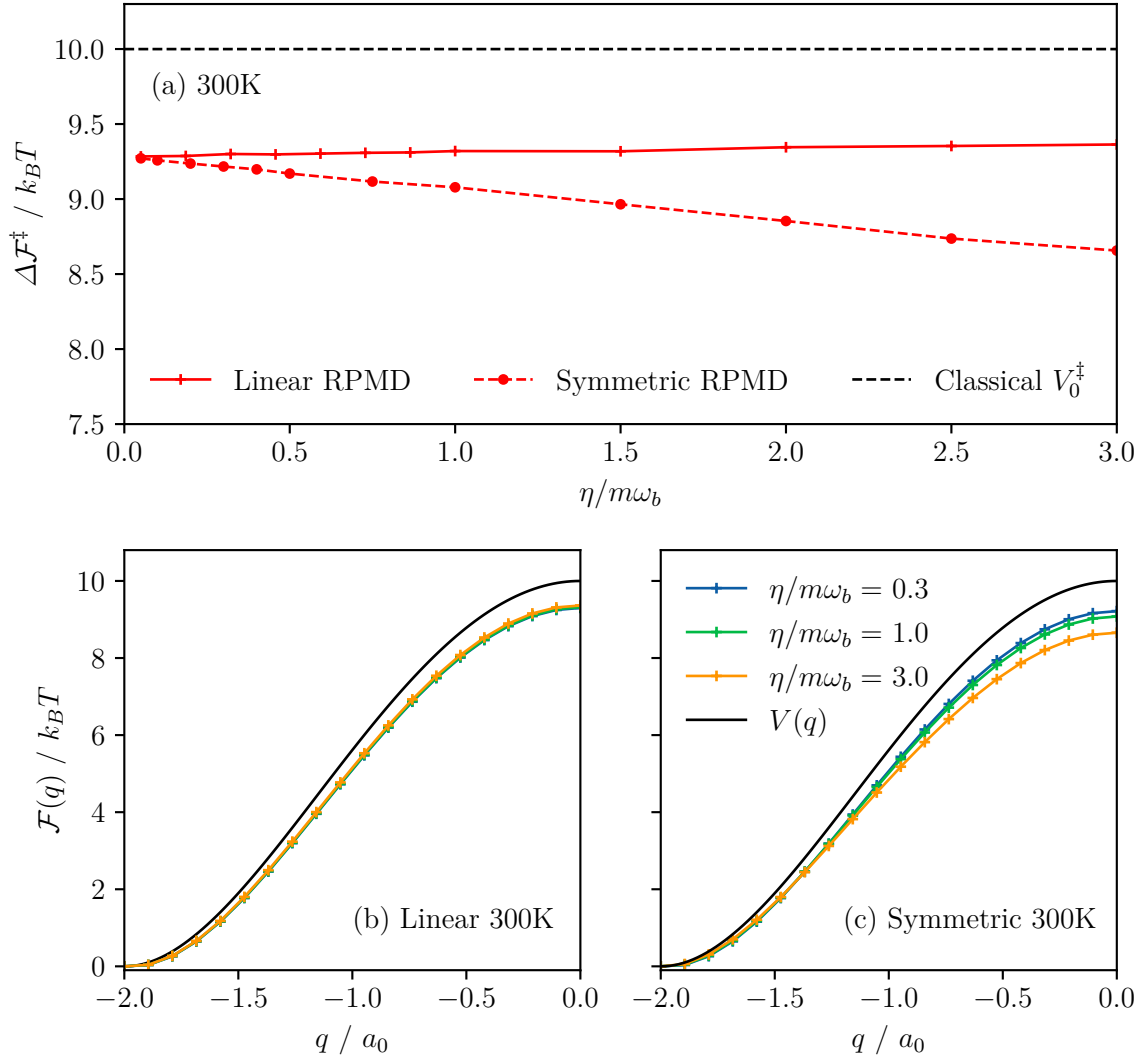
Fig. 4.4 Free energy barriers at $T = 300$K, plotted for the linear (solid red) and symmetric (dashed red) RPMD calculations. The analytic value for the classical free energy barrier ($V_0^{\ddagger} = 10\ k_B T$) is added for reference. Panels (b) and (c) show plots of the barriers as a function of the reaction coordinate, q, for three values of $\eta/m\omega_b$.

The key difference is that the symmetric model shows a distinct *decrease* in barrier height for higher values of $\eta/m\omega_b$, whereas the barrier in the linear regime slowly increases towards the classical limit as $\eta/m\omega_b \to \infty$. The following section presents results for a further investigation into this effect of the nonlinear friction on the local free energies in the reactant well and at the transition state.

4.2.2 Free Energy Description

To elucidate the behaviour of the symmetric free energy barrier seen in Fig. 4.4, the free energy changes from introducing nonlinearity were computed in the reactant well and at the transition state, by performing a thermodynamic integration upon varying the value of ϵ in the coupling function $g(q; \epsilon)$. With the resulting values, it is possible to construct the thermodynamic cycle in Fig. 4.5.
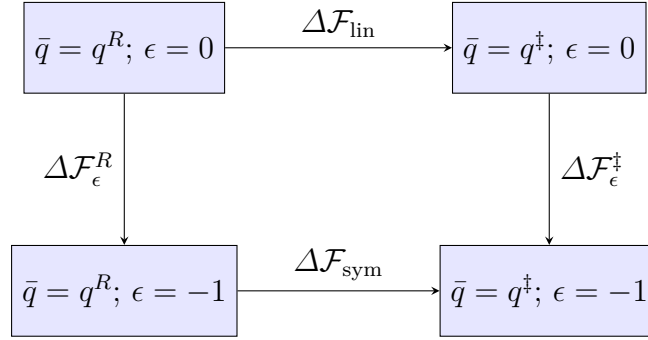

Fig. 4.5 Thermodynamic cycle for interpolation between linear and symmetric friction regimes for a particular value of $\eta/m\omega_b$. The values q^R and $q^\ddagger$ refer to the centroid reaction coordinate of the bottom of the reactant well and the dividing surface, respectively.

The cycle satisfies the relationship:

$$\Delta\mathcal{F}_{\text{lin}} = \Delta\mathcal{F}_\epsilon^R + \Delta\mathcal{F}_{\text{sym}} - \Delta\mathcal{F}_\epsilon^\ddagger, \tag{4.8}$$

where the free energy differences $\Delta\mathcal{F}_{\text{lin}}$ and $\Delta\mathcal{F}_{\text{sym}}$ are those computed at 300K as part of the rate calculations. The vertical arrows in Fig. 4.5 were calculated as[†]:

$$\Delta\mathcal{F}_\epsilon = \int_{-1}^0 d\epsilon \left\langle \frac{1}{N} \sum_{j=1}^N \frac{\partial V(q_j; \epsilon)}{\partial \epsilon} \right\rangle_{\epsilon,\, \bar{q}=q}, \tag{4.9}$$

where the integrand is a centroid-constrained RPMD thermal average for a given value of ϵ and $\bar{q}$ (q^R or $q^\ddagger$). The derivative of the ring polymer potential with respect to ϵ is given by

$$\frac{\partial V(q_j; \epsilon)}{\partial \epsilon} = -\sum_{i=1}^{N_b} \left(x_{i,j} - \frac{f_i(q_j; \epsilon)}{m_i \omega_i^2} \right) \frac{\partial f_i(q_j; \epsilon)}{\partial \epsilon}, \tag{4.10}$$

where

$$\frac{\partial f_i(q_j; \epsilon)}{\partial \epsilon} = c_i q_j \sqrt{\eta} \exp\left(-q_j^2/2\right). \tag{4.11}$$

[†]See Appendix C.3 for the full method of thermodynamic integration.

Results obtained for the thermodynamic cycle with $\eta/m\omega_b = 3$ are given in Table 4.1, which show that interpolating from linear to symmetric friction results in an *increase* in free energy in the reactant well and a *decrease* at the dividing surface.

$\Delta\mathcal{F}_{\text{lin}}$	+9.36 k_BT	$\Delta\mathcal{F}_\epsilon^R$	+0.29 k_BT
$\Delta\mathcal{F}_{\text{sym}}$	+8.66 k_BT	$\Delta\mathcal{F}_\epsilon^\ddagger$	-0.41 k_BT

Table 4.1 Free energy differences at $T = 300$K for the thermodynamic cycle, with $\eta/m\omega_b = 3$. Values are numerically converged to 2 decimal places, and satisfy Equation (4.8).

The local free energies change as a consequence of the changing local friction upon varying ϵ; an increase in friction results in an increase in free energy and vice-versa, which is consistent with the simple harmonic picture discussed in Chapter 3. The barrier behaviour in Fig. 4.4 can therefore be described in terms of the reactant and transition state free energies, since free energy is a state function.

In the linear regime, the friction is position-independent, so stronger coupling raises the free energy approximately equal amounts everywhere, such that the barrier increases slowly towards the classical limit as $\eta/m\omega_b \to \infty$.

For symmetric friction, increasing $\eta/m\omega_b$ only strengthens the coupling in the wells, since there is zero friction at the dividing surface. The reactant free energy therefore increases with coupling strength while the transition state free energy remains unchanged, resulting in a lowering of the barrier and consequently a systematic increase in the rate seen in Fig. 4.2. A depiction of this effect on the free energy is shown in Fig. 4.6.
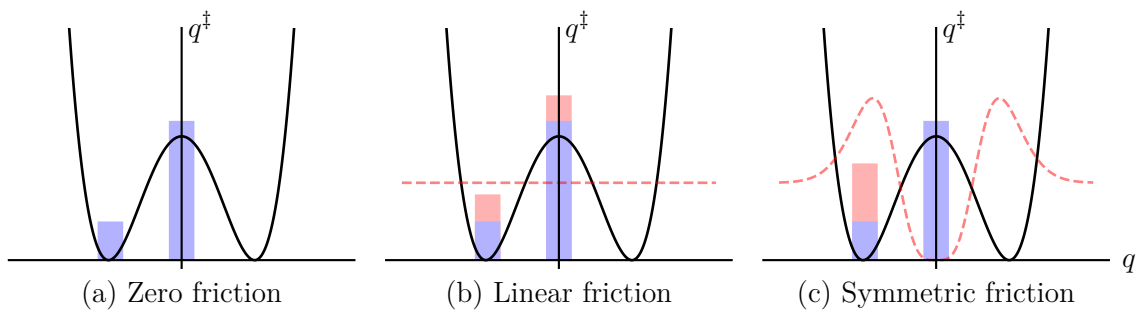

(a) Zero friction (b) Linear friction (c) Symmetric friction

Fig. 4.6 Schematic diagram of the behaviour of the reactant and transition state quantum free energies for linear and symmetric friction at $T = 300$K. Panel (a) represents the free energies in the absence of any system-bath coupling. Panels (b) and (c) illustrate how the free energies are changed with increasing friction in the linear and symmetric regimes.

The continuous decrease of the barrier height is a product of the symmetric model exerting *zero* friction at the barrier for all $\eta/m\omega_b$, such that the system will never reach the classical limit. This model is a limiting case that was chosen to accentuate the effects of nonlinearity; in real systems there would be always non-zero barrier friction[†].

4.2.3 Deep-Tunnelling Regime

Rates were also computed at 50K to examine the behaviour of the position-dependent friction model below the instanton crossover temperature, T_c, where the reaction becomes dominated by deep tunnelling. It is known that the RPMD rate constant in this regime is equivalent to an approximate version of semiclassical instanton theory[3], which explains why RPMD is able to yield good estimates for the quantum rate at low temperatures. Results for linear and symmetric friction are shown in Fig. 4.7.
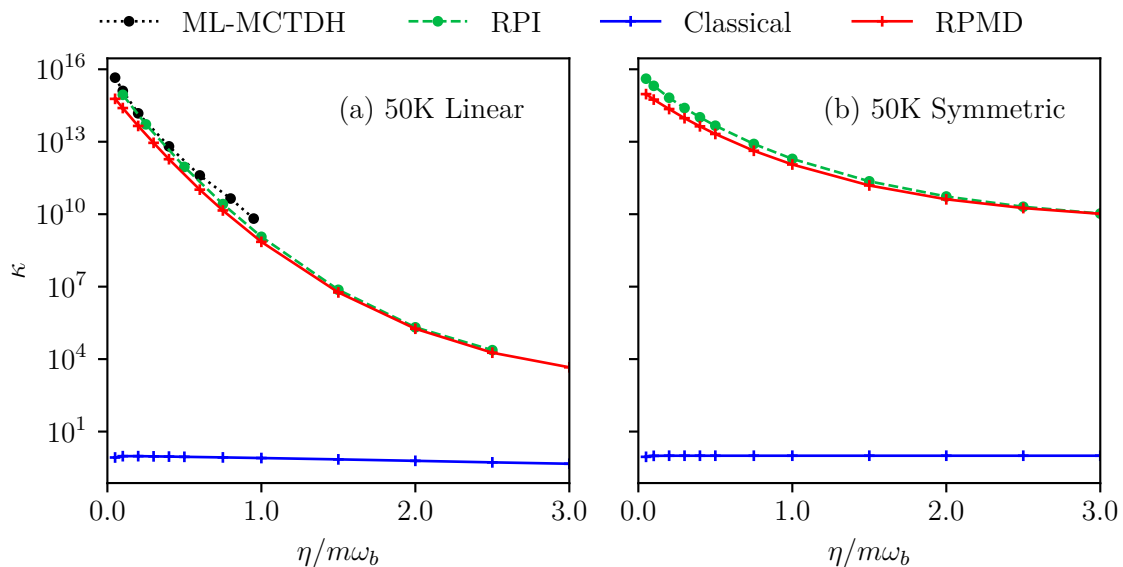

Fig. 4.7 Dimensionless rate constants at $T = 50$K. Panel (a) shows the linear friction regime and panel (b) shows the symmetric friction regime. Results from exact quantum dynamics (ML-MCTDH) and ring polymer instanton theory (RPI) from Ref. [26] have been included for comparison. The RPMD results were found to be fully converged for $N = 64$ beads.

The RPMD rates are vastly greater than the classical rates, highlighting how classical MD completely fails when deep-tunnelling is present at low temperatures. The results show good agreement with ring polymer instanton (RPI) calculations taken from a recent low-temperature study of the same system[26], with a maximum difference of a factor of 3 for the lowest value of $\eta/m\omega_b$. The linear RPMD rates also perform well

[†]See Appendix E.2 for calculations with finite friction at the barrier, by taking $\epsilon = -0.25$.

compared to exact quantum dynamics simulations from multilayer multi-configuration time-dependent Hartree theory (ML-MCTDH)[48], taken from the same reference; the maximum difference is a factor of 6, which is promising for a much less expensive method. The RPMD results in this work are now being used by the authors of these benchmark results to assist in producing ML-MCTDH rates for nonlinear system-bath coupling.

In contrast to 300K, the rates for both friction regimes systematically decrease with increasing $\eta/m\omega_b$. This is due to delocalisation of the ring polymer at low temperature, which can be seen by noting the significant deviation of the dynamics from classical behaviour in the transmission factors in Figs. 4.8 (a) and (b). The bead springs are sufficiently loose for $T < T_c$ that the ring polymer becomes delocalised and no longer acts as a compact body with classical-like dynamics.

It has previously been shown[18] that increasing bath friction shifts T_c downwards due to contraction of the ring polymer from the bath renormalisation potential discussed in Chapter 3. This dominates the behaviour of the free energy barriers, as is shown in Figs. 4.8 (c), (d) and (e).

Deep-tunnelling barriers were observed to have a 'flat top' shape due to the ring polymer delocalisation, which captures this dominant tunnelling pathway and has been observed previously in low-temperature RPMD studies[49]. The downward shift in T_c with stronger coupling brings the ring polymer closer to the edge of the deep-tunnelling regime, which can be seen in Fig. 4.8 (d), where the free energy profiles clearly change from the flat shape to the familiar barrier shape seen at 300K, producing a significant barrier increase. In the symmetric regime, the lack of friction at the transition state means that the bath is poorer at contracting the ring polymer and thus there is a much smaller shift in T_c with varying coupling strength. This results in a slower increase in the barrier than with the linear case, explaining why the symmetric model has been observed to yield faster rates.
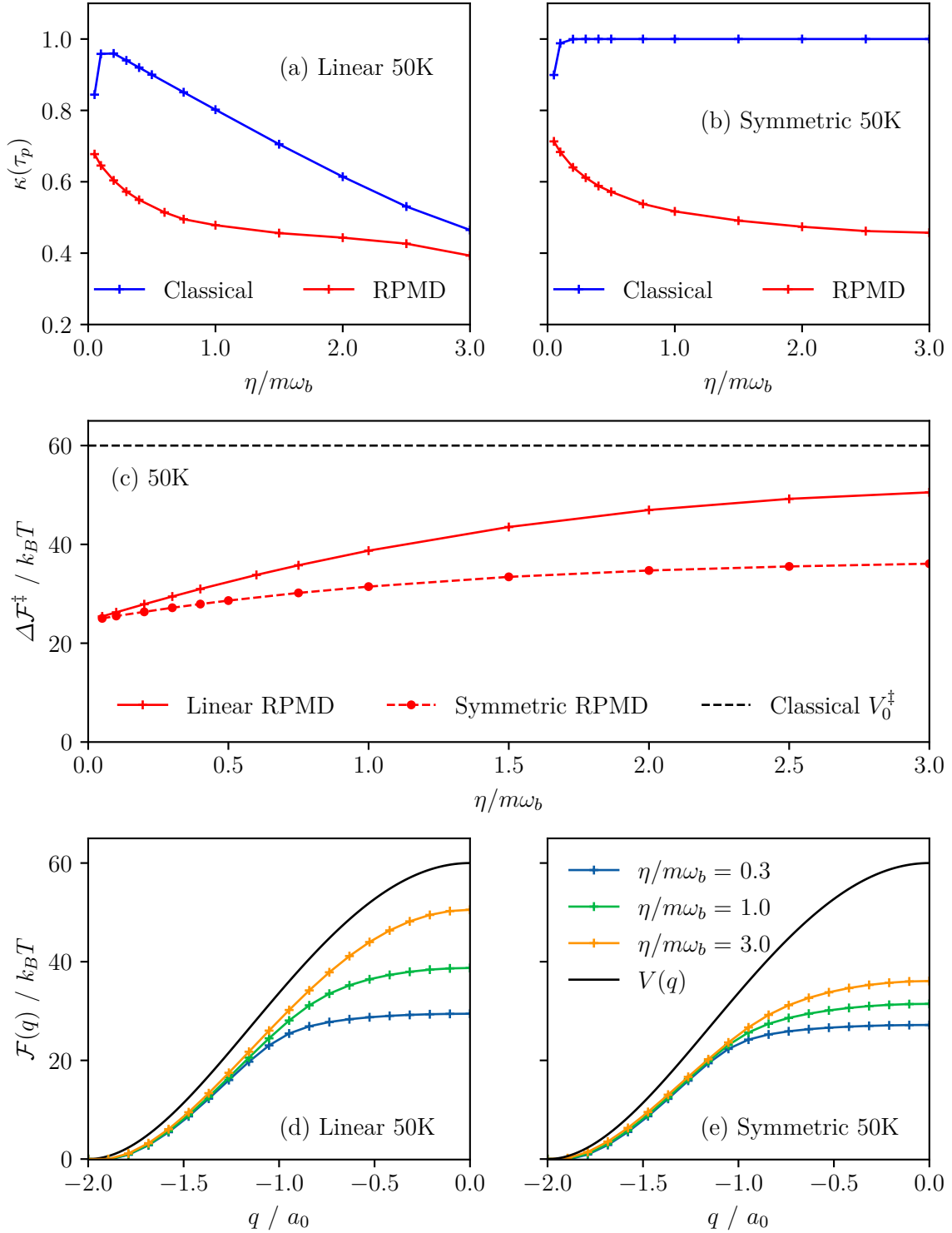
Fig. 4.8 Transmission coefficients and free energy barriers at $T = 50$K. Panels (a) and (b) show the classical and quantum dynamical behaviour of the linear and symmetric models, respectively. Panel (c) displays the general trend for the linear and symmetric free energy barriers as the bath coupling strength is varied. Plots of the barriers for three selected values of η are shown in panels (d) and (e).

Chapter 5

Application to Hydrogen Hopping in Bulk Palladium

5.1 Model

To apply the nonlinear system-bath model to a more physically realistic system, in this chapter we consider hydrogen diffusion in bulk palladium. Specifically, the process of interest is the migration from an octahedral to a tetrahedral interstitial site (O→T) within the face-centred cubic (fcc) lattice. Data for the minimum energy pathway (MEP) and a series of *ab initio* spectral density tensors taken at 14 points along the reaction path were obtained from Refs. [26, 50] to form a one-dimensional nonlinear system-bath.

The migration path of hydrogen was found to be linear, but a reactive event also involves distortion of the palladium atoms. To account for this, the system was mapped onto a set of values, $\{q_1, \ldots, q_n\}$, of a one-dimensional mass-weighted reaction coordinate:

$$q_\alpha = \sum_{\alpha'=1}^{\alpha-1} \sqrt{\sum_{\beta=1}^{f} m_j (r_{\alpha'+1,\beta} - r_{\alpha',\beta})^2}, \tag{5.1}$$

for a set of position vectors in f-dimensional configuration space, $\{\mathbf{r}_1, \ldots, \mathbf{r}_n\}$, where each vector $\mathbf{r}_\alpha$ represents a nuclear geometry at a point along the MEP. These values formed the reaction coordinate, q, that was used as the position variable for the system-bath model. The spectral density tensors, computed for the three hydrogen degrees of freedom, were projected onto the path taken by hydrogen:

$$J(\mathbf{q}, \omega) = \frac{1}{|\mathbf{R}|^2} \sum_{ij}^{f} R_i \, J_{ij}(\mathbf{q}, \omega) \, R_j, \tag{5.2}$$

where $\mathbf{R}$ is the tangent vector to the reaction path for a given hydrogen position, $\mathbf{q}$.
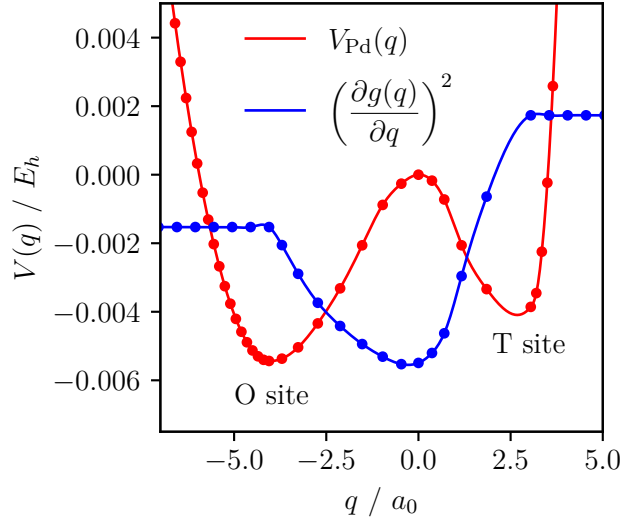
Fig. 5.1 Mass-weighted MEP (red) for the diffusion of hydrogen from an octahedral to a tetrahedral interstitial site. The plot of $(g'(q))^2$ (blue, arbitrary units) has been calculated from *ab initio* spectral density data.

The bath frequencies $\{\omega_i\}$ and coupling function $g(q)$ were determined from the 1D spectral densities by the discretisation method of Walters *et al.*[46][†]. To complete the model, harmonic approximations using the relevant normal mode frequency were employed on either end of the reactant and product wells. The friction in these approximated regions was taken to be constant. The MEP and position-friction profile are given in Fig. 5.1.

To examine the importance of nonlinear coupling when calculating the rate for this process, results are compared with a corresponding linear system-bath, where the position-independent friction was set to the value at the transition state, $q^{\ddagger}$:

$$J(q^{\ddagger}, \omega) \rightarrow J(\omega). \tag{5.3}$$

5.2 Rate Calculations

Classical and RPMD rate constants for the hydrogen hopping reaction were calculated at $T = 300$K using the Bennett-Chandler method. Results were computed using the palladium spectral density with both the O→T MEP and the DW1 model potential, to observe the how the potential energy surface (PES) affects the interplay of NQEs and NAEs. Position-independent rates were also computed as described above.

Similarly to Chapter 5, the rates have been normalised by the classical TST rate *of the corresponding PES*, to give a dimensionless value, κ. In the case of the palladium

---

[†]See Appendix D.1 for the full bath discretisation method.

O→T MEP, the harmonic approximation employed in Equation (4.7) yields a poor estimate of $k_{\text{cl}}^{\text{TST}}(T)$ due to significant anharmonicity in the reactant well. For this potential, the TST rate was instead calculated numerically using the method outlined in Chapter 2 with $N = 1$. Results for the two potentials are given in Tables 5.1 and 5.2.

$V_{\text{DW1}}(q)$	Position-Independent		Position-Dependent	
	MD	RPMD	MD	RPMD
Rate, κ	0.193(3)	0.357(4)	0.315(5)	0.582(7)
$\kappa(\tau_p)$	0.193(3)	0.184(2)	0.315(5)	0.299(2)
$\Delta\mathcal{F}^{\ddagger} / k_B T$	9.999*	9.286(2)	9.999*	9.283(2)

Table 5.1 Classical and RPMD normalised rate constants, transmission factors and free energy barriers at $T = 300$K, simulated with the Pd spectral density and the DW1 potential. Values in brackets are standard error estimates of the final digit. Values with a (*) are equal to the potential energy barrier, $V_0^{\ddagger}$.

$V_{\text{Pd}}(q)$	Position-Independent		Position-Dependent	
	MD	RPMD	MD	RPMD
Rate, κ	0.180(3)	0.211(3)	0.429(3)	0.498(2)
$\kappa(\tau_p)$	0.180(3)	0.180(2)	0.429(3)	0.410(4)
$\Delta\mathcal{F}^{\ddagger} / k_B T$	5.723*	5.577(6)	5.723*	5.546(4)

Table 5.2 Classical and RPMD normalised rate constants, transmission factors and free energy barriers at $T = 300$K, simulated with the Pd spectral density and the Pd O→T mass-weighted MEP. Values with a (*) are equal to the MEP potential energy barrier.

Numerical calculations for the DW1 potential in Table 5.1 show comparable changes in the rate when including NQEs compared to including position-dependent friction, both of which yield an increase by a factor of 1.5-2.0. For the palladium O→T MEP, the most significant change in the rate comes from the position-dependent friction (around a factor of 2.5), with only a small increase from including NQEs (a factor of 1.2). At 300K, Fig. 5.2 shows that the free energy barrier for hydrogen migration is only marginally smaller than the potential barrier, resulting in only a small correction
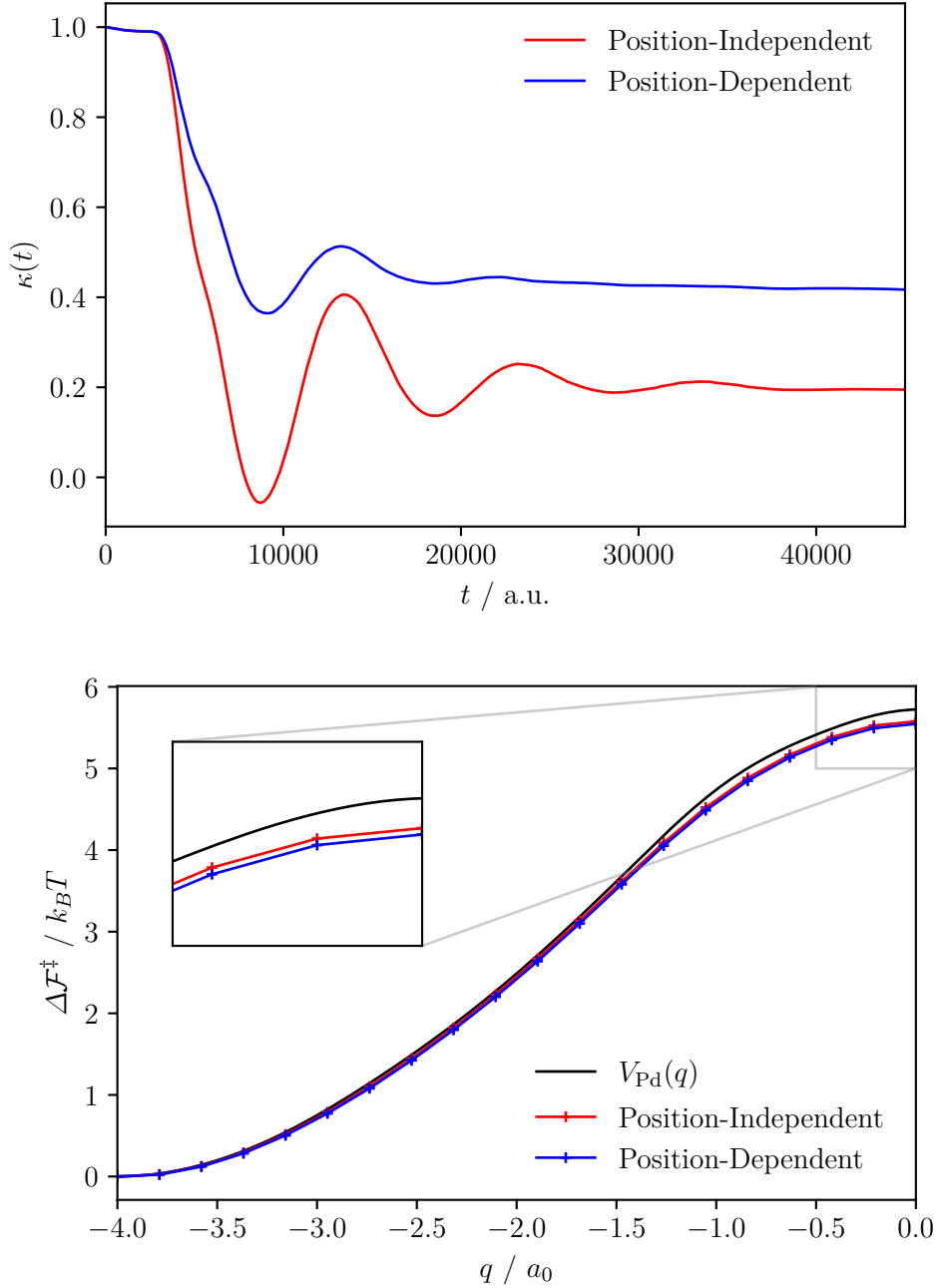
Fig. 5.2 Transmission factors and free energy barriers for hydrogen O→T migration in Pd for the position-independent (red) and position-dependent (blue) friction models, with the O→T mass-weighted MEP (black).

to the rate from NQEs. It is also observed from Fig. 5.2 that the increase in the rate for position-dependent friction is almost entirely due to the dynamics; the barrier heights for both cases only differ by a very small amount. However, the nonlinear friction profile is significantly affecting the recrossing dynamics, which are behaving almost classically at this temperature. The somewhat surprising lack of NQEs present for this system has
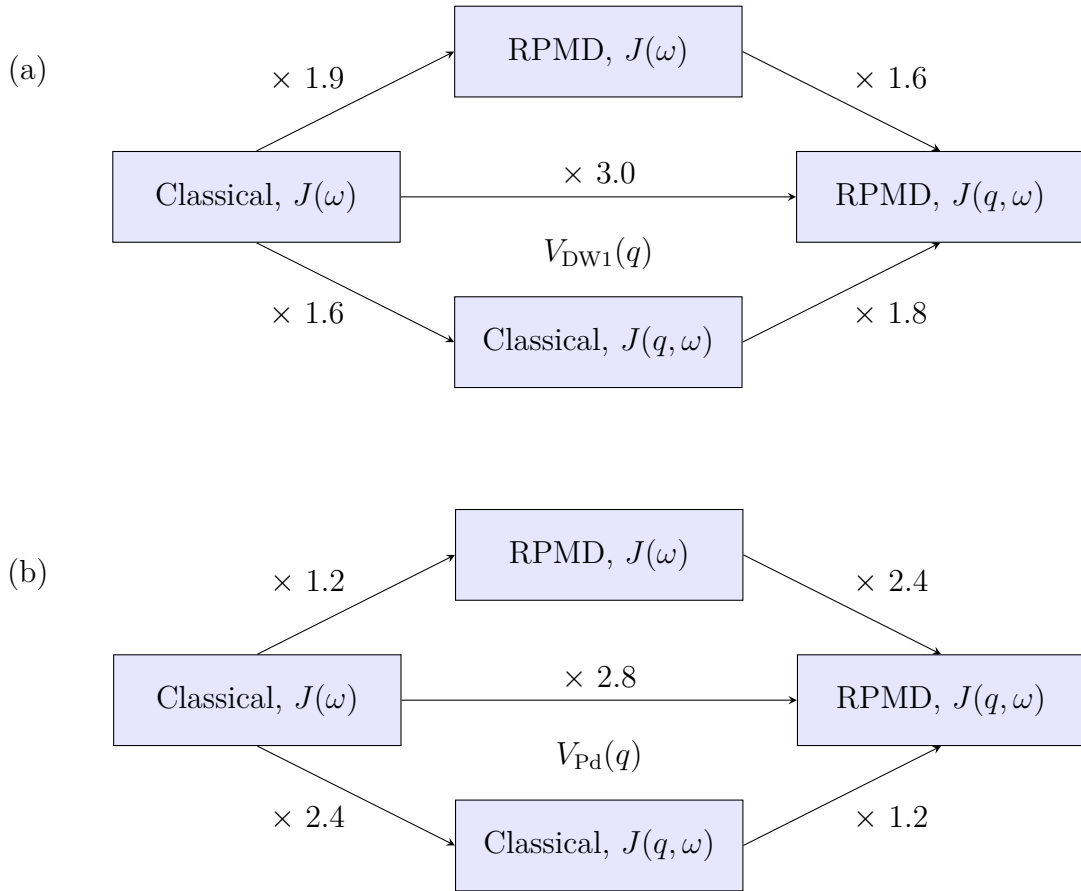
Fig. 5.3 Summary of rate increase factors for a nonlinear system-bath with the Pd spectral density, applied to (a) the DW1 potential and (b) the Pd O→T mass-weighted MEP.

been attributed to two factors. Firstly, the mass-weighting of the reaction coordinate results in a longer effective path which is producing a free energy barrier closer to the classical limit than if the reaction coordinate was simply taken to be the hydrogen path. Secondly, our one-dimensional model is not able to capture multidimensional NQEs which have been found to *increase* the barrier in this system[51].

The diagram in Fig. 5.3 summarises the relative increases in the rate for the DW1 and palladium MEP potentials when introducing quantum effects and nonlinear coupling to the bath. Overall, we report that the inclusion of position-dependent friction to account for NAEs in metallic systems is important as it is seen to have an effect of comparable, if not greater magnitude than the inclusion of NQEs.

Chapter 6

Conclusions and Further Work

In this work, a nonlinear system-bath model was developed to compute rate coefficients with classical molecular dynamics and ring polymer molecular dynamics (RPMD)[12]. The model was applied to a one-dimensional double well potential at 300K and 50K, for a range of bath friction strengths, and extended to hydrogen hopping between palladium interstitial sites, by taking a projection of the position-dependent *ab initio* spectral density tensor along the reaction coordinate.

At 300K, numerical results show that position-dependent friction significantly alters the recrossing dynamics which behave classically due to the compact nature of the ring polymers. Additionally, quantum effects on the rate are observed for strong coupling, since the bath contribution to the free energy becomes strongly dependent on position.

In the deep-tunnelling regime, RPMD rates for linear and nonlinear coupling were found to be in good agreement with recent ring polymer instanton (RPI) calculations[26], and numerically exact results from multilayer multi-configuration time-dependent Hartree theory (ML-MCTDH)[26,48]. A lowering of the crossover temperature with friction was observed to heavily impact the free energy barriers for both linear and nonlinear coupling.

Results for hydrogen hopping in palladium at 300K showed that the nonlinear coupling is too weak to show any quantum effects from the inclusion of position-dependent friction. Nevertheless, the change in the recrossing dynamics yields a greater effect on the rate than accounting for nuclear quantum effects, highlighting the importance of considering spatially-dependent non-adiabatic effects when simulating metallic systems.

Routes for further research include studying hydrogen diffusion in palladium in full dimensionality, so we are able to account for additional multidimensional nuclear quantum effects which have been observed[51]. Additionally, we aim to utilise the general model applied to palladium for the simulation of real systems that exhibit different friction profiles, to gain a more complete picture of the behaviour of quantum dynamics in nonlinear dissipative environments.

Appendices

Appendix A

Ring Polymers as Imaginary-Time Path Integrals

The quantum mechanical propagator, $U(q, t; q_0, 0) = \langle q|e^{-i\hat{H}t/\hbar}|q_0 \rangle$, can be written as an integral over all paths between q_0 and q, with each path weighted by its classical action[33]:

$$U(q, t; q_0, 0) = \int_{\substack{q(t)=q \\ q(0)=q_0}} \mathcal{D}q(t) \, \exp\left(\frac{iS[q(t)]}{\hbar}\right), \tag{A.1}$$

where the action, $S[q(t)]$, and the integration variable are defined as

$$S[q(t)] = \int_0^t \mathrm{d}t' \, \left[\frac{m}{2}\left(\frac{\mathrm{d}q}{\mathrm{d}t'}\right)^2 - V(q)\right], \tag{A.2}$$

$$\int \mathcal{D}q(t) = \lim_{N\to\infty} \left(\frac{Nm}{2\pi\hbar i t}\right)^{N/2} \int \mathrm{d}q_1 \ldots \mathrm{d}q_{N-1}. \tag{A.3}$$

Writing Equation (A.1) in discrete form, with $\delta t = t/N$, yields the expression

$$\begin{aligned}
U(q, t; q_0, 0) = \lim_{\substack{N\to\infty \\ \delta t\to 0}} &\left(\frac{m}{2\pi\hbar i\delta t}\right)^{N/2} \int \mathrm{d}q_1 \ldots \mathrm{d}q_{N-1} \\
&\times \exp\left(\frac{i\delta t}{\hbar} \sum_{j=0}^{N-1} \left[\frac{m}{2}\left(\frac{q_j - q_{j+1}}{\delta t}\right)^2 - V(q_j)\right]\right).
\end{aligned} \tag{A.4}$$

The quantum partition function expressed in position space can be written in terms of the propagator with $t = -i\beta\hbar$ and $q_0 = q$:

$$Z = \int \mathrm{d}q \, \langle q|e^{-\beta\hat{H}}|q \rangle = \int \mathrm{d}q \, U(q, -i\beta\hbar; q, 0). \tag{A.5}$$

To proceed, consider a transformation to imaginary time, $\tau = it$, where $\tau = \beta\hbar$. It follows that $i\delta t = \beta\hbar/N = \beta_N\hbar$. The condition $q = q_0$ can be achieved by introducing the cyclic boundary conditions $q_j \equiv q_{N+j}$. Equation (A.4) can therefore be rewritten as

$$U(q, -i\beta\hbar; q, 0) = \lim_{N \to \infty} \left(\frac{m}{2\pi\beta_N\hbar^2} \right)^{N/2} \int dq_1 \dots dq_{N-1}$$
$$\times \exp\left(-\beta_N \sum_{j=0}^{N-1} \left[\frac{m}{2\beta_N^2\hbar^2}(q_j - q_{j+1})^2 + V(q_j) \right] \right). \tag{A.6}$$

Recognising the form of the ring polymer Hamiltonian[7,12], integrating Equation (A.6) with respect to q and expressing the prefactor as an integral over momenta yields the familiar result:

$$Z = \lim_{N \to \infty} \frac{1}{(2\pi\hbar)^N} \int d\mathbf{p} \int d\mathbf{q} \, e^{-\beta_N H_N(\mathbf{p},\mathbf{q})}. \tag{A.7}$$

It follows that a ring polymer with finite N is equivalent to a discrete cyclic imaginary-time path integral where each bead represents a snapshot in imaginary time. In the infinite-bead limit, the partition function may be written as a continuous imaginary-time path integral:

$$Z = \int dq \oint \mathcal{D}q(\tau) \exp\left(-\frac{S[q(\tau)]}{\hbar} \right). \tag{A.8}$$

Appendix B

Bennett-Chandler Method

B.1 Derivation of RPMD Transition State Theory

A one-dimensional system is considered in this derivation, where the dividing surface is given by $\bar{s}(\mathbf{q}) = q^{\ddagger} - \bar{q}$; the following analysis may be easily generalised to higher dimensional systems. As $t \to 0$, the $h(\bar{q}(t) - q^{\ddagger})$ term in the flux-side TCF will become $h(\bar{p})$, since the initial momentum of the ring polymer centroid will determine whether it is moving into the reactant or product region[4]. The zero-time limit of $\widetilde{C}_{fs}^{(N)}(t)$ is written as

$$\lim_{t \to 0^+} \widetilde{C}_{fs}^{(N)}(t) = \frac{1}{(2\pi\hbar)^N} \int d\mathbf{p} \int d\mathbf{q} \, e^{-\beta_N H_N(\mathbf{p},\mathbf{q})} \delta(q^{\ddagger} - \bar{q})(\bar{p}/m)h(\bar{p}). \tag{B.1}$$

This can be separated into a product of two integrals; one over the momenta and one over the positions[29]:

$$\lim_{t \to 0^+} \widetilde{C}_{fs}^{(N)}(t) = \frac{1}{(2\pi\hbar)^N} \int d\mathbf{p} \, \exp\left(-\beta_N \sum_{j=1}^{N} \frac{p_j^2}{2m}\right) (\bar{p}/m)h(\bar{p})$$

$$\times \int d\mathbf{q} \, \exp\left(-\beta_N \sum_{j=1}^{N} \left[\frac{1}{2}m\omega_N^2(q_j - q_{j+1})^2 + V(q_j)\right]\right) \delta(q^{\ddagger} - \bar{q}). \tag{B.2}$$

The integral over the momenta is evaluated as follows:

$$I_p = \int dp_1 \ldots dp_N \, \exp\left(-\beta_N \sum_{j=1}^{N} \frac{p_j^2}{2m}\right) \frac{\bar{p}}{m}h(\bar{p}). \tag{B.3}$$

Transforming to the ring polymer normal mode basis, and using the fact that the momentum centroid $\bar{p} = P_0/\sqrt{N}$, the integral becomes

$$I_p = \int dP_0 \ldots dP_{N-1} \, \exp\left(-\beta_N \sum_{k=0}^{N-1} \frac{P_k^2}{2m}\right) \frac{P_0}{m\sqrt{N}} \, h(P_0). \tag{B.4}$$

Factorising the exponential term into its individual components, the integral for the non-centroid modes is

$$\int_{-\infty}^{\infty} dP_k \, \exp\left(-\beta_N \frac{P_k^2}{2m}\right) = \left(\frac{2\pi m}{\beta_N}\right)^{1/2} \qquad k > 0. \tag{B.5}$$

For the centroid mode, the Heaviside step function causes all negative momenta to contribute zero to the integral, so one can express the integral over positive momenta only:

$$\int_0^{\infty} dP_0 \, \exp\left(-\beta_N \frac{P_0^2}{2m}\right) \frac{P_0}{m\sqrt{N}} = \frac{1}{\beta_N \sqrt{N}}$$

$$\tag{B.6}$$

$$= \frac{1}{(2\pi\beta m)^{1/2}} \left(\frac{2\pi m}{\beta_N}\right)^{1/2}.$$

Combining the contributions from all of the normal modes, I_p becomes

$$I_p = \frac{1}{(2\pi\beta m)^{1/2}} \left(\frac{2\pi m}{\beta_N}\right)^{N/2}$$

$$\tag{B.7}$$

$$= \frac{1}{2}\langle|\dot{q}|\rangle_{cl} \int d\mathbf{p} \, \exp\left(-\beta_N \sum_{j=1}^{N} \frac{p_j^2}{2m}\right),$$

where the former term is the purely classical flux through the dividing surface, and the latter term has been re-expressed as a Gaussian integral over the momenta of all beads. Substituting this result back into Equation (B.2) yields:

$$\lim_{t\to 0^+} \widetilde{C}_{fs}^{(N)}(t) = \frac{1}{2}\langle|\dot{q}|\rangle_{cl} \frac{1}{(2\pi\hbar)^N} \int d\mathbf{p} \int d\mathbf{q} \, e^{-\beta_N H_N(\mathbf{p},\mathbf{q})} \delta(q^{\ddagger} - \bar{q})$$

$$\tag{B.8}$$

$$= \frac{1}{2}\langle|\dot{q}|\rangle_{cl} Q^{(N)}(q^{\ddagger}),$$

where $Q^{(N)}(q^{\ddagger})$ is the centroid-constrained partition function. The transition state theory rate constant can be written as

$$k^{\text{QTST}}(T) = \frac{1}{2}\langle|\dot{q}|\rangle_{cl} \frac{Q^{(N)}(q^{\ddagger})}{Q_r^{(N)}(T)} = \frac{1}{2}\langle|\dot{q}|\rangle_{cl} \frac{\langle\delta(q^{\ddagger} - \bar{q})\rangle}{\langle h(q^{\ddagger} - \bar{q})\rangle}. \tag{B.9}$$

A useful result from this analysis is found by comparing Equation (B.9) with Equation (B.1):

$$\langle \delta(q^{\ddagger} - \bar{q})(\bar{p}/m)h(\bar{p})\rangle = \frac{1}{2}\langle|\dot{q}|\rangle_{\mathrm{cl}}\langle\delta(q^{\ddagger} - \bar{q})\rangle. \tag{B.10}$$

For a higher dimensional system, where the dividing surface is given by $\bar{s}(\mathbf{q}) = q_s^{\ddagger} - \bar{q}_s$, the results are the same since the integrals over all the other degrees of freedom become included in the $Q^{(N)}(q_s^{\ddagger})$ term.

B.2 Mean Force

Here we derive the relationship between the free energy $\mathcal{F}$ and the mean force defined in Section 3.2. We start with the following relationships:

$$\frac{\mathrm{d}}{\mathrm{d}\bar{q}} = \sqrt{N}\frac{\partial}{\partial Q_0} = \sqrt{N}\sum_{j=1}^{N}C_{j0}\frac{\partial}{\partial q_j} = \sum_{j=1}^{N}\frac{\partial}{\partial q_j}, \tag{B.11}$$

$$\sum_{j=1}^{N}\frac{1}{2}m\omega_N^2\left(q_j - q_{j-1}\right)^2 = \sum_{k=0}^{N-1}\frac{1}{2}m\omega_k^2 Q_k^2, \tag{B.12}$$

which follow from the normal mode transformation $\mathbf{Q} = \mathbf{C}^{\top}\mathbf{q}$. Note that Equation (B.12) shows that the ring polymer spring terms are independent of the centroid mode, since $\omega_0 = 0$. Now starting with the definition of the free energy $\mathcal{F}(q)$:

$$\mathcal{F}(q) = -\frac{1}{\beta}\ln p(q). \tag{B.13}$$

Taking the derivative of $\mathcal{F}$ with respect to q yields

$$\frac{\mathrm{d}\mathcal{F}(q)}{\mathrm{d}q} = -\frac{1}{\beta p(q)}\frac{\mathrm{d}p(q)}{\mathrm{d}q}. \tag{B.14}$$

By writing $p(q)$ as in Equation (2.19), the free energy derivative can be written as

$$\frac{\mathrm{d}\mathcal{F}(q)}{\mathrm{d}q} = -\frac{1}{2\pi\hbar\beta\langle\delta(q-\bar{q})\rangle}\int\mathrm{d}\mathbf{p}\int\mathrm{d}\mathbf{q}\,\mathrm{e}^{-\beta_N H_N(\mathbf{p},\mathbf{q})}\frac{\mathrm{d}}{\mathrm{d}q}\delta(q-\bar{q})$$

$$\tag{B.15}$$

$$= -\frac{1}{2\pi\hbar\beta\langle\delta(q-\bar{q})\rangle}\int\mathrm{d}\mathbf{p}\int\mathrm{d}\mathbf{q}\,\delta(q-\bar{q})\frac{\mathrm{d}}{\mathrm{d}\bar{q}}\mathrm{e}^{-\beta_N H_N(\mathbf{p},\mathbf{q})}.$$

Using the relationships from Equations (B.11) and (B.12):

$$\frac{\mathrm{d}\mathcal{F}(q)}{\mathrm{d}q} = \frac{1}{2\pi\hbar\beta\langle\delta(q-\bar{q})\rangle} \int \mathrm{d}\mathbf{p} \int \mathrm{d}\mathbf{q}\, \delta(q-\bar{q}) \left[\beta_N \sum_{j=1}^{N} \frac{\partial V(q_j)}{\partial q_j}\right] \mathrm{e}^{-\beta_N H_N(\mathbf{p},\mathbf{q})}$$

$$= \frac{1}{2\pi\hbar\langle\delta(q-\bar{q})\rangle} \int \mathrm{d}\mathbf{p} \int \mathrm{d}\mathbf{q} \left[\frac{1}{N} \sum_{j=1}^{N} \frac{\partial V(q_j)}{\partial q_j}\right] \mathrm{e}^{-\beta_N H_N(\mathbf{p},\mathbf{q})} \delta(q-\bar{q}) \qquad (\mathrm{B.16})$$

$$= \left\langle \frac{1}{N} \sum_{j=1}^{N} \frac{\partial V(q_j)}{\partial q_j} \right\rangle_{\bar{q}=q}.$$

Thus the free energy derivative can be evaluated by performing constrained centroid simulations with $\bar{q} = q$. By performing a series of simulations for different values of q, one can calculate $\mathcal{F}(q)$ via a simple thermodynamic integration.

Appendix C

Semiclassical Langevin Dynamics

Here we present a derivation of the nuclear Langevin equation with electronic friction, which follows that of Dou *et al.*[44] Assuming semiclassical dynamics, the nuclear degrees of freedom, $(\mathbf{p}, \mathbf{q})$, and the electronic density matrix, $\hat{\rho}(t)$, respectively obey Hamilton's equations and the von Neumann equation:

$$-m_i \ddot{q}_i = \partial_i \hat{H}, \tag{C.1}$$

$$\frac{\mathrm{d}\hat{\rho}}{\mathrm{d}t} = -\hat{\hat{\mathcal{L}}}\hat{\rho}, \tag{C.2}$$

where $\partial_i \equiv \partial/\partial q_i$ and $\hat{\hat{\mathcal{L}}}(\cdot) = \frac{i}{\hbar}\left[\hat{H}, \cdot\right]$ is the Liouvillian superoperator. Rewriting Equation (C.1) in terms of an average force and random force gives the following form:

$$-m_i \ddot{q}_i = \mathrm{Tr}_e\left[\partial_i \hat{H}\hat{\rho}\right] + \left(\partial_i \hat{H} - \mathrm{Tr}_e\left[\partial_i \hat{H}\hat{\rho}\right]\right), \tag{C.3}$$

where $\mathrm{Tr}_e\left[\,\cdot\,\right]$ is a trace over the electronic degrees of freedom. In this derivation, it is assumed that the electronic degrees of friction relax on much faster timescales than the nuclei. During a small time Δt, in which nucleus i moves a distance of $\dot{q}_i \Delta t$, the small deviation from the steady state electronic density matrix is given by:

$$\hat{\rho} = \hat{\rho}_{ss} + \Delta\hat{\rho} \implies \frac{\mathrm{d}\hat{\rho}}{\mathrm{d}t} = -\hat{\hat{\mathcal{L}}}\Delta\hat{\rho}. \tag{C.4}$$

Assuming $\Delta\hat{\rho}$ to be small, it can be approximated using $\hat{\rho} \approx \hat{\rho}_{ss}$:

$$\Delta\hat{\rho} \simeq -\hat{\hat{\mathcal{L}}}^{-1}\frac{\mathrm{d}\hat{\rho}_{ss}}{\mathrm{d}t}$$

$$= \sum_j \dot{q}_j \hat{\hat{\mathcal{L}}}^{-1}\partial_j\hat{\rho}_{ss}, \tag{C.5}$$

where in the second line the chain rule has been applied. Substituting this result into Equation (C.3) yields a Langevin equation for the semiclassical dynamics:

$$-m_i \ddot{q}_i = -F_i + \sum_j \eta_{ij} \dot{q}_j - \delta \hat{F}_i, \tag{C.6}$$

where the mean force, friction kernel and random force are defined, respectively, as follows:

$$F_i = -\text{Tr}_e \left[\partial_i \hat{H} \hat{\rho}_{ss} \right], \tag{C.7}$$

$$\eta_{ij} = -\text{Tr}_e \left[\partial_i \hat{H} \hat{\mathcal{L}}^{-1} \partial_j \hat{\rho}_{ss} \right], \tag{C.8}$$

$$\delta \hat{F}_i = -\partial_i \hat{H} + \text{Tr}_e \left[\partial_i \hat{H} \hat{\rho}_{ss} \right]. \tag{C.9}$$

To obtain the time-dependent friction tensor, $\eta_{ij}(\mathbf{q}, t)$, the following identity for the inverse of the Liouvillian is used[44]:

$$\hat{\mathcal{L}}^{-1} = -\lim_{\epsilon \to 0^+} \int_0^\infty \mathrm{d}t \, \mathrm{e}^{-(\hat{\mathcal{L}} + \epsilon)t}. \tag{C.10}$$

Substituting this into the friction kernel expression of Equation (C.8), and noting the parallels with the classical Langevin equation static friction[30], $\eta_0 = \int_0^\infty \mathrm{d}t \, \eta(t)$, the dynamic friction tensor is identified as

$$\eta_{ij}(\mathbf{q}, t) = -\text{Tr}_e \left[\partial_i \hat{H} \mathrm{e}^{-i\hat{\mathcal{L}}t} \partial_j \hat{\rho}_{ss} \right]. \tag{C.11}$$

Appendix D

Computational Details

D.1 Explicit Determination of Bath Parameters

The determination of the bath parameters follows the 'logarithmic' discretisation method proposed by Walters *et al.*[46], which gives all the bathmodes the same fraction of the reorganisation energy. This leads to frequency-dependent coefficients of the form:

$$c_i = \kappa \sqrt{m_i} \omega_i, \tag{D.1}$$

where κ is a constant. Thus, by noting that $c_i^2/m_i\omega_i^2 = \kappa^2 \ \forall \ i$, the spectral density of Equation (3.4) divided by ω can be written as

$$\frac{J(q,\omega)}{\omega} = \frac{\pi}{2} \left(\kappa \frac{\partial g(q)}{\partial q} \right)^2 \sum_{i=1}^{N_b} \delta(\omega - \omega_i). \tag{D.2}$$

For the palladium spectral density in Chapter 5, the *ab initio* data[26,50] produced multiple frequency-dependent spectral density plots for varying q. For each fixed value of q, the quantity $\epsilon(q)$ is calculated to determine the value of $\kappa g'(q)$ using the following relationship:

$$\epsilon(q) = \frac{1}{N_b} \int_0^\infty \mathrm{d}\omega \frac{J(q,\omega)}{\omega} = \frac{\pi}{2} \left(\kappa \frac{\partial g(q)}{\partial q} \right)^2. \tag{D.3}$$

For computational simplicity, the value of κ is absorbed into the definition of the position-dependent function without changing the equations of motion; the new coefficient and friction function are defined as

$$\tilde{c}_i = \sqrt{m_i} \omega_i \qquad \tilde{g}(q) = \kappa g(q), \tag{D.4}$$

such that $\tilde{g}'(q) = \sqrt{2\epsilon(q)/\pi}$.

This gives the same value for the system-bath interaction in the Hamiltonian, $f_i(q)$:

$$f_i(q) = c_i g(q) = \tilde{c}_i \tilde{g}(q). \tag{D.5}$$

The discrete $\tilde{g}(q)$ values were then used to form a smooth differentiable spline for use in the integration scheme. The bath frequencies $\{\omega_i\}$ are calculated as follows, choosing the value of q to be that of the transition state, $q^{\ddagger}$:

$$\frac{1}{\epsilon(q^{\ddagger})} \int_0^{\omega_i} \mathrm{d}\omega \, \frac{J(q^{\ddagger}, \omega)}{\omega} = \int_0^{\omega_i} \mathrm{d}\omega \sum_{i=1}^{N_b} \delta(\omega - \omega_i) = i - \frac{1}{2}. \tag{D.6}$$

In theory, the bath frequencies should take the same values for all q, however this relies on the separable approximation, $f_i(q) = \tilde{c}_i \tilde{g}(q)$. In reality, for the *ab initio* calculations the coupling is not exactly separable, but it is still a good approximation. It can also be shown[46] that this discretisation method gives rise to the coefficients and frequencies of the well-known Ohmic bath with an exponential cut-off, which are used in Chapter 4:

$$c_i = \omega_i \sqrt{\frac{2 m_i \omega_c}{\pi N_b}} \qquad \omega_i = -\omega_c \ln\left(\frac{i - 1/2}{N_b}\right). \tag{D.7}$$

D.2   Integration Scheme

The ring polymer Hamiltonian in Equation (3.2) can be separated into a free ring polymer Hamiltonian and an external potential term[35]:

$$H_N(\mathbf{p}, \mathbf{q}, \mathbf{p}_b, \mathbf{x}) = H_0(\mathbf{p}, \mathbf{q}, \mathbf{p}_b, \mathbf{x}) + V_N(\mathbf{q}, \mathbf{x}), \tag{D.8}$$

where

$$H_0(\mathbf{p}, \mathbf{q}, \mathbf{p}_b, \mathbf{x}) = \sum_{j=1}^{N} \left[\frac{p_j^2}{2\mu} + \frac{1}{2}\mu\omega_N^2 \left(q_j - q_{j+1}\right)^2 \right] + \sum_{i=1}^{N_b}\sum_{j=1}^{N} \left[\frac{p_{i,j}^2}{2m_i} + \frac{1}{2}m_i\omega_N^2 \left(x_{i,j} - x_{i,j+1}\right)^2 \right], \tag{D.9}$$

and

$$V_N(\mathbf{q}, \mathbf{x}) = \sum_{j=1}^{N} V(q_j) + \sum_{i=1}^{N_b}\sum_{j=1}^{N} \left[\frac{1}{2}m_i\omega_i^2 \left(x_{i,j} - \frac{f_i(q_j)}{m_i\omega_i^2} \right)^2 \right]. \tag{D.10}$$

The time dependence of the system depends on the Liouvillian, $\mathcal{L}_N$[30], which can also be split into two terms:

$$\mathcal{L}_N = \mathcal{L}_0 + \mathcal{L}_V. \tag{D.11}$$

This system can be evolved in time using the following symmetric-split propagator[35]:

$$\mathrm{e}^{-\mathcal{L}\Delta t} \simeq \mathrm{e}^{-\mathcal{L}_V \Delta t/2}\mathrm{e}^{-\mathcal{L}_0 \Delta t}\mathrm{e}^{-\mathcal{L}_V \Delta t/2}, \tag{D.12}$$

which can be implemented using the following velocity Verlet[39] scheme for even N:

$$p_j \leftarrow p_j - \frac{\Delta t}{2}\frac{\partial V_N(\mathbf{q})}{\partial q_j}$$

$$P_k \leftarrow \sum_{j=1}^{N} p_j C_{jk} \qquad Q_k \leftarrow \sum_{j=1}^{N} q_j C_{jk}$$

$$\begin{pmatrix} P_k \\ Q_k \end{pmatrix} \leftarrow \begin{pmatrix} \cos\omega_k\Delta t & -m\omega_k\sin\omega_k\Delta t \\ (1/m\omega_k)\sin\omega_k\Delta t & \cos\omega_k\Delta t \end{pmatrix}\begin{pmatrix} P_k \\ Q_k \end{pmatrix} \tag{D.13}$$

$$p_j \leftarrow \sum_{k=0}^{N-1} C_{jk} P_k \qquad q_j \leftarrow \sum_{k=0}^{N-1} C_{jk} Q_k$$

$$p_j \leftarrow p_j - \frac{\Delta t}{2}\frac{\partial V_N(\mathbf{q})}{\partial q_j},$$

with $\omega_k = 2\omega_N \sin(k\pi/N)$. The orthogonal normal mode transformation matrix C_{jk} is defined in Section 1.3. For position dependent friction, the external momentum updates were performed by taking the derivative of the external potential $V_N(\mathbf{q})$ with respect to the system and bath degrees of freedom respectively:

$$\frac{\partial V_N(\mathbf{q}, \mathbf{x})}{\partial q_j} = \frac{\partial V(q_j)}{\partial q_j} - \sum_{i=1}^{N_b} x_{i,j}\frac{\partial f_i(q_j)}{\partial q_j} + \sum_{i=1}^{N_b} \frac{f_i(q_j)}{m_i\omega_i^2}\frac{\partial f_i(q_j)}{\partial q_j}, \tag{D.14}$$

$$\frac{\partial V_N(\mathbf{q}, \mathbf{x})}{\partial x_{i,j}} = m_i\omega_i^2 x_{i,j} - f_i(q_j). \tag{D.15}$$

D.3   Thermodynamic Integration

This section outlines the method of thermodynamic integration[30], which has been used frequently in this work for the calculation of free energy differences. Consider an f-dimensional classical Hamiltonian with a potential that depends on a parameter λ:

$$V(\mathbf{q}; \lambda) = (1 - \lambda)V_A(\mathbf{q}) + \lambda V_B(\mathbf{q}). \tag{D.16}$$

In this case, by continuously changing λ from $0 \rightarrow 1$, the system adiabatically interpolates from state A with potential V_A, to state B with potential V_B. The classical partition

function is given by

$$Z_{\text{cl}}(\lambda) = \frac{1}{(2\pi\hbar)^f} \int d\mathbf{p} \int d\mathbf{q} \, \exp\left(-\beta\left[\sum_{i=1}^{f} \frac{p_i^2}{2m_i} + V(\mathbf{q};\lambda)\right]\right), \qquad \text{(D.17)}$$

and the Helmholtz free energy is related to the partition function with the following expression:

$$\mathcal{F}(\lambda) = -\frac{1}{\beta} \ln Z_{\text{cl}}(\lambda). \qquad \text{(D.18)}$$

To obtain an expression for a free energy difference on changing λ, it is instructive to take the derivative with respect to λ:

$$\frac{\partial \mathcal{F}}{\partial \lambda} = -\frac{1}{\beta Z_{\text{cl}}} \frac{\partial Z_{\text{cl}}}{\partial \lambda}$$

$$= -\frac{1}{\beta} \frac{\int d\mathbf{p} \int d\mathbf{q} \left(-\beta \frac{\partial V}{\partial \lambda}\right) e^{-\beta H(\mathbf{p},\mathbf{q};\lambda)}}{\int d\mathbf{p} \int d\mathbf{q} \, e^{-\beta H(\mathbf{p},\mathbf{q};\lambda)}} \qquad \text{(D.19)}$$

$$= \left\langle \frac{\partial V}{\partial \lambda} \right\rangle_\lambda.$$

Thus the free energy derivative can be computed from a thermal average of a derivative of the potential evaluated for a certain value of λ. It follows that the free energy difference can be obtained from a definite integral:

$$\Delta \mathcal{F}_{AB} = \int_0^1 d\lambda \, \frac{\partial \mathcal{F}}{\partial \lambda}$$

$$\qquad \text{(D.20)}$$

$$= \int_0^1 d\lambda \, \left\langle \frac{\partial V}{\partial \lambda} \right\rangle_\lambda.$$

For RPMD simulations, applying this analysis to the ring polymer classical extended phase space yields the following expression for the free energy derivative:

$$\frac{\partial \mathcal{F}}{\partial \lambda} = \left\langle \frac{1}{N} \sum_{j=1}^{N} \frac{\partial V(q_j)}{\partial \lambda} \right\rangle_\lambda. \qquad \text{(D.21)}$$

D.4   Simulation Details

The simulation parameters for the numerical rate calculations are provided in Tables D.1 and D.2. The number of beads, N, number of bathmodes, N_b, and number of sample trajectories were all converged to within graphical accuracy. The timestep, Δt, was taken to be 5% of the period of the highest frequency bathmode[15]. For all simulations of equilibrium quantities such as free energies, and for initial thermalisation of a trajectory, an Andersen thermostat was used where the bead momenta were periodically resampled from the Boltzmann distribution, $e^{-\beta_N H_N}$, every 50 timesteps.

The number of samples taken varied for the different components of the rate (transmission factors, centroid-constrained mean forces and reactant well simulations); all components were converged within 10^5 samples.

	Linear		Symmetric	
	300K	50K	300K	50K
N	16	64	16	64
N_b	9	9	12	12
Δt / a.u.	47.7	47.7	43.4	43.4
$\tau_p/\Delta t$	190	190	190	190

Table D.1 Parameters used for simulations of the system-bath model with the DW1 potential in Chapter 4.

$T = 300$K	Position-Independent		Position-Dependent	
	DW1	Pd	DW1	Pd
N	16	16	16	16
N_b	96	96	96	96
Δt / a.u.	17.6	17.6	17.6	17.6
$\tau_p/\Delta t$	2600	2600	2600	2600

Table D.2 Parameters used for simulations of the Pd O→T migration reaction in Chapter 5, with the DW1 potential and Pd minimum energy pathway.

Appendix E

Supplementary Data

E.1   Position Distributions

The effect of the nonlinear system-bath model on the system position distribution was investigated by computing histograms of centroid positions for the two friction regimes studied in the previous sections. To accentuate the difference in behaviour between the linear and nonlinear models, a steep 'box-like' potential, $V(q) = aq^{12}$, where $a = 3.068 \times 10^{-9}$, was used (the value of a was chosen such that the potential was of the same width as the DW1 potential).
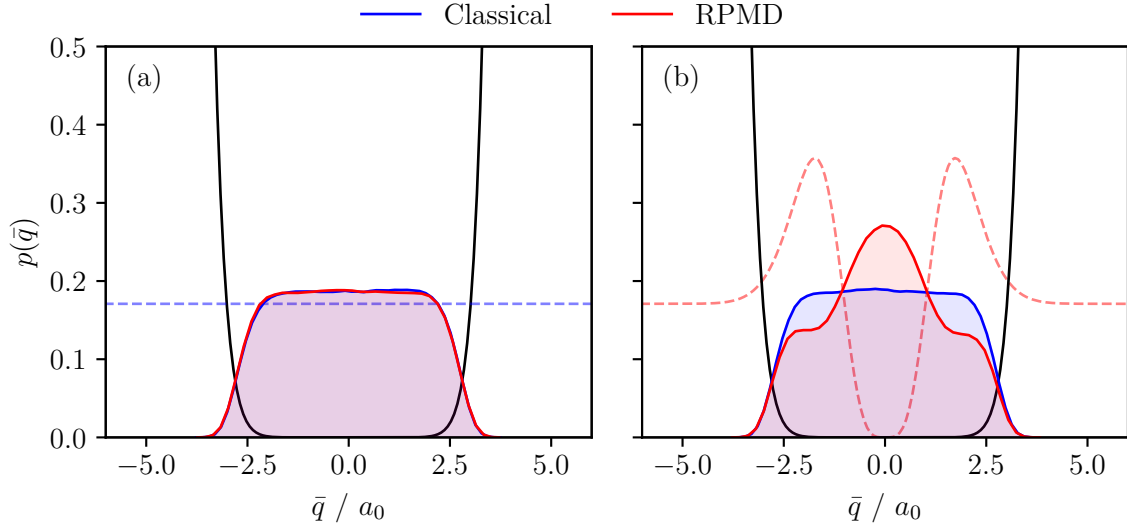

Fig. E.1 Classical and RPMD centroid position distributions for (a) linear and (b) symmetric friction, for the 'box-like' potential, $V(q) = aq^{12}$, with $a = 3.068 \times 10^{-9}$ and $T = 300$K. Schematic depictions of the position-dependence of the friction are shown on the respective plots as a dashed line.

Classical and linear RPMD distributions all behave the same, with a 'uniform' distribution within the well. However, the RPMD distribution under symmetric friction clearly shows a skew towards the area of low friction. The ring polymer lowers its free energy by being localised in the low friction region. Friction-driven localisation is a nuclear quantum effect, and assists the idea of the nonlinear friction profile lowering the free energy barrier, as seen in Chapter 4.

E.2   Intermediate Nonlinear Friction

An intermediate value for the parameter ϵ in the coupling function $g(q; \epsilon)$ used in Chapter 4 was taken to examine the relationship between the linear and symmetric friction regimes. Results for the RPMD rate constant κ at $T = 300$K are shown in Fig. E.2 along with the corresponding linear and symmetric values.
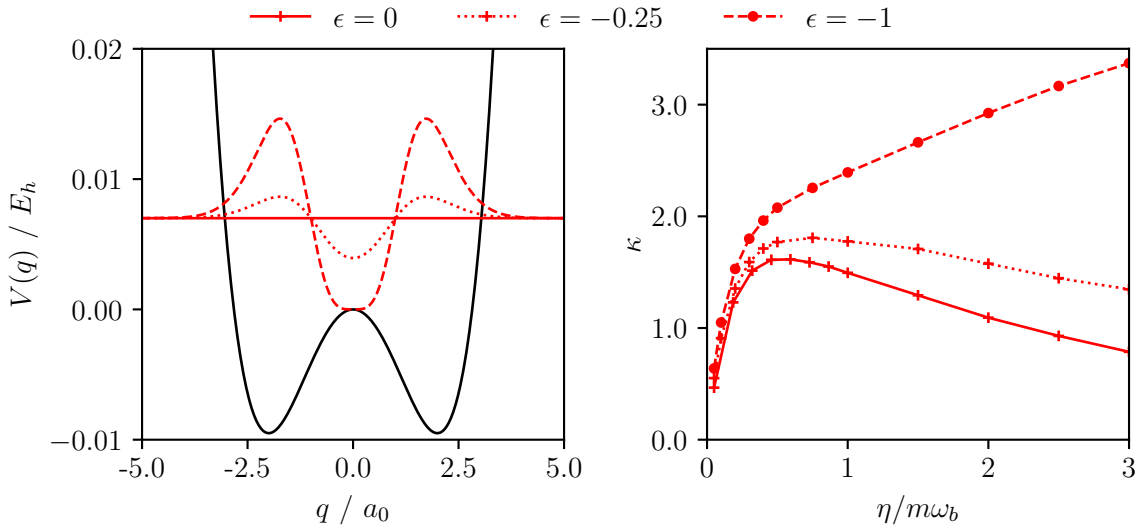

Fig. E.2 DW1 potential with friction profiles for three values of ϵ, and corresponding RPMD rates at $T = 300$K. The rates for $\epsilon = 0$ (solid red) and $\epsilon = -1$ (dashed red) are those calculated for linear and symmetric friction in Chapter 4. The intermediate value of $\epsilon = -0.25$ (dotted red) is added to show how these limiting regimes are related. The y-values for the friction profiles are arbitrary.

It is clear to see that even a small amount of nonlinearity in the friction profile is yielding faster rates than the nonlinear case, which is consistent with the description of the free energies and recrossing dynamics discussed in Chapter 4.

Bibliography

[1] S. Habershon and D. E. Manolopoulos, J. Chem. Phys. **131**, 244518 (2009).

[2] W. H. Miller, J. Chem. Phys. **125**, 132305 (2006).

[3] J. O. Richardson and S. C. Althorpe, J. Chem. Phys. **131**, 214106 (2009).

[4] R. Collepardo-Guevara, I. R. Craig, and D. E. Manolopoulos, J. Chem. Phys. **128**, 144502 (2008).

[5] Y. V. Suleimanov, R. Collepardo-Guevara, and D. E. Manolopoulos, J. Chem. Phys. **134**, 044131 (2011).

[6] T. F. Miller and D. E. Manolopoulos, J. Chem. Phys. **122**, 184503 (2005).

[7] M. Parrinello and A. Rahman, J. Chem. Phys. **80**, 860–867 (1984).

[8] D. Marx and M. Parrinello, J. Chem. Phys. **104**, 4077 (1998).

[9] H. Wang, M. Thoss, K. L. Sorge, R. Gelabert, X. Giménez, and W. H. Miller, J. Chem. Phys. **114**, 2562–2571 (2001).

[10] J. Cao and G. A. Voth, J. Chem. Phys. **100**, 5106–5117 (1994).

[11] S. Jang and G. A. Voth, J. Chem. Phys. **111**, 2371–2384 (1999).

[12] I. R. Craig and D. E. Manolopoulos, J. Chem. Phys. **121**, 3368–3373 (2004).

[13] T. J. H. Hele, M. J. Willatt, A. Muolo, and S. C. Althorpe, J. Chem. Phys. **142**, 134103 (2015).

[14] T. J. H. Hele, M. J. Willatt, A. Muolo, and S. C. Althorpe, J. Chem. Phys. **142**, 191101 (2015).

[15] I. R. Craig and D. E. Manolopoulos, J. Chem. Phys. **122**, 084106 (2005).

[16] J. O. Richardson, J. Chem. Phys. **144**, 114106 (2016).

[17] C. Bartels, R. Cooper, D. J. Auerbach, and A. M. Wodtke, Chem. Sci. **2**, 1647–1655 (2011).

[18] Y. Litman, E. S. Pós, C. L. Box, R. Martinazzo, R. J. Maurer, and M. Rossi, J. Chem. Phys. **156**, 194106 (2022).

[19] M. Askerka, R. J. Maurer, V. S. Batista, and J. C. Tully, Phys. Rev. Lett. **116**, 217601 (2016).

[20] C. L. Box, Y. Zhang, R. Yin, B. Jiang, and R. J. Maurer, J. Am. Chem. Soc. Au. **1**, 164–173 (2021).

[21] R. J. Maurer, M. Askerka, V. S. Batista, and J. C. Tully, Phys. Rev. B **94**, 115432 (2016).

[22] A. O. Caldeira and A. J. Leggett, Ann. Phys. **149**, 374–456 (1983).

[23] G. A. Voth, J. Chem. Phys. **97**, 5908–5910 (1992).

[24] G. R. Haynes and G. A. Voth, J. Chem. Phys. **103**, 10176–10182 (1995).

[25] G. R. Haynes, G. A. Voth, and E. Pollak, J. Chem. Phys. **101**, 7811–7822 (1994).

[26] Y. Litman, E. S. Pós, C. L. Box, R. Martinazzo, R. J. Maurer, and M. Rossi, J. Chem. Phys. **156**, 194107 (2022).

[27] R. Feynman and A. Hibbs, *Quantum Mechanics and Path Integrals: Emended Edition* (Dover Publications, 2010).

[28] D. Chandler and P. G. Wolynes, J. Chem. Phys. **74**, 4078–4095 (1981).

[29] I. R. Craig and D. E. Manolopoulos, J. Chem. Phys. **123**, 034102 (2005).

[30] M. E. Tuckerman, *Statistical Mechanics: Theory and Molecular Simulation* (Oxford University Press, 2010).

[31] J. J. Sakurai and J. Napolitano, *Modern Quantum Mechanics: Third Edition* (Cambridge University Press, 2017).

[32] A. Nitzan, *Chemical Dynamics in Condensed Phases: Relaxation, Transfer, and Reactions in Condensed Molecular Systems* (Oxford University Press, 2006).

[33] R. Shankar, *Principles of Quantum Mechanics* (Plenum Press, 1994).

[34] R. Kubo, J. Phys. Soc. Jpn. **12**, 570–586 (1957).

[35] M. Ceriotti, M. Parrinello, T. E. Markland, and D. E. Manolopoulos, J. Chem. Phys. **133**, 124104 (2010).

[36] W. H. Miller, J. Chem. Phys. **61**, 1823–1834 (1974).

[37] W. H. Miller, S. D. Schwartz, and J. W. Tromp, J. Chem. Phys. **79**, 4889–4898 (1983).

[38] D. Chandler, J. Chem. Phys. **68**, 2959–2970 (1978).

[39] D. Frenkel and B. Smit, *Understanding Molecular Simulation: From Algorithms to Applications* (Academic Press, 2002).

[40] G. R. Haynes, G. A. Voth, and E. Pollak, Chem. Phys. Lett. **207**, 309–316 (1993).

[41] E. Pollak, J. Chem. Phys. **85**, 865–867 (1986).

[42] M. Head-Gordon and J. C. Tully, J. Chem. Phys. **103**, 10137–10145 (1995).

[43] Y. V. Nazarov and J. Danon, *Advanced Quantum Mechanics: A Practical Guide* (Cambridge University Press, 2013).

[44] W. Dou, G. Miao, and J. E. Subotnik, Phys. Rev. Lett. **119**, 046001 (2017).

[45] M. Topaler and N. Makri, J. Chem. Phys. **101**, 7500–7519 (1994).

[46] P. L. Walters, T. C. Allen, and N. Makri, J. Comput. Chem. **38**, 110–115 (2017).

[47] H. A. Kramers, Physica **7**, 284–304 (1940).

[48] H. Wang and M. Thoss, J. Chem. Phys. **119**, 1289–1299 (2003).

[49] J. R. Cendagorta, A. Powers, T. J. H. Hele, O. Marsalek, Z. Bačić, and M. E. Tuckerman, Phys. Chem. Chem. Phys. **18**, 32169–32177 (2016).

[50] Y. Litman, Private communication.

[51] H. Kimizuka, S. Ogata, and M. Shiga, Phys. Rev. B **100**, 024104 (2019).